The Thesis Committee for Navid Ghorashian
Certifies that this is the approved version of the following thesis:

Parallelized Microfluidic Devices for High-Throughput Nerve Regeneration Studies in *Caenorhabditis Elegans*

APPROVED BY
SUPERVISING COMMITTEE:

Supervisor:

Adela Ben-Yakar

Jon Pierce-Shimomura

Parallelized Microfluidic Devices for High-Throughput Nerve Regeneration Studies in *Caenorhabditis Elegans*

by

Navid Ghorashian, B.A.

Thesis

Presented to the Faculty of the Graduate School of

The University of Texas at Austin

in Partial Fulfillment

of the Requirements

for the Degree of

Master of Science in Engineering

The University of Texas at Austin

August 2010

Dedication

I would like to dedicate this thesis to the people closest to me. My mother's influence could only be equaled by a higher power. My father has grown to be a solid rock in my life. My uncle brought joy to my childhood and continues to be a close friend. My step-mother gave me guidance in the very basic and important aspects of life. My little brothers and sister have taught me how to love unconditionally. My aunt is full of humor and spirit. My close friends from childhood through graduate school have become like family. Thank you all for letting me be a part of your lives.

Acknowledgements

I would like to thank Dr. Frank Werblin at UC Berkeley for giving me my first research position as an undergrad and allowing me to learn first hand what rigorous scientific research demands; religious dedication. Dr. Luke P. Lee of UC Berkeley also gave me the opportunity to perform research as an undergrad, and it is in his lab that I developed confidence in my creativity and passion for research. Dr. Adela Ben-Yakar of UT Austin has brought me into her group with open arms, and has allowed me pursue a wide breath of my scientific interests in the project described here. Her passion and enthusiasm for multidisciplinary research has been infectious and I thank her for her continued support and guidance. Dr. Massimo Hilliard of the Queensland Brain Institute has been an excellent mentor in the biological aspects of this project. Dr. Jon Pierce-Shimomura at UT Austin has also been very helpful in my understanding of *C. elegans* neurobiology and has been very generous with his time and mentorship. My fellow lab members, past and present, have been instrumental to the progress of this project and are all excellent human beings: Sam Xun Guo, Frederic Bourgeois, Neil Everett, Elaine Ellerton, Sigfried Haering, Nick Durr, Chris Hoy, Rick Harrison, and Daniel Eversole.

Abstract

Parallelized Microfluidic Devices for High-Throughput Nerve Regeneration Studies in *Caenorhabditis Elegans*

Navid Ghorashian, M.S.E.

The University of Texas at Austin, 2010

Supervisor: Adela Ben-Yakar

The nexus of engineering and molecular biology has given birth to high-throughput technologies that allow biologists and medical scientists to produce previously unattainable amounts of data to better understand the molecular basis of many biological phenomena. Here, we describe the development of an enabling biotechnology, commonly known as microfluidics in the fabrication of high-throughput systems to study nerve degeneration and regeneration in the well-defined model nematode, *Caenorhabditis elegans* (*C. elegans*). Our lab previously demonstrated how femtosecond (fs) laser pulses could precisely cut nerve axons in *C. elegans,* and we observed axonal regeneration *in vivo* in single worms that were immobilized on anesthetic treated agar pads. We then developed a microfluidic device capable of immobilizing one worm at a time with a deformable membrane to perform these experiments without agar pads or anesthetics. Here, we describe the development of improved microfluidic devices that can trap and

immobilize up to 24 individual worms in parallel chambers for high-throughput axotomy and subsequent imaging of nerve regeneration in a single platform. We tested different micro-channel designs and geometries to optimize specific parameters: (1) the initial trapping of a single worm in each immobilization chamber, simultaneously, (2) immobilization of single worms for imaging and fs-laser axotomy, and (3) long term storage of worms on-chip for imaging of regeneration at different time points after the initial axon cut.

Table of Contents

List of Tables

List of Figures

Chapter 1: Introduction

The potential impact of understanding the underlying molecular and genetic mechanisms of nerve regeneration and degeneration would have profound benefits to human health. Severe disorders of the central nervous system (e.g. Alzheimer's and Parkinson's), as well as injuries (e.g. spinal cord damage and stroke) are some of the most devastating ailments known to modern medicine. A major step towards enhancing fundamental knowledge of these conditions would be to elucidate their mechanisms in well-understood *in vivo* systems [1].

In 2004, our group demonstrated the use of femtosecond (fs) laser pulses to precisely cut nerve axons in the roundworm, *Caenorhabditis elegans* (*C. elegans*) and observed that these axons can regenerate shortly after nano-surgery [2]. With this laser and the proper optical setup, one can ablate (photo-disrupt) femtoliter volumes with sub-micron spatial precision, while causing minimum damage to surrounding tissue. Concurrently, the use *C. elegans* as a model organism facilitates nerve regeneration and degeneration studies due to its fully characterized neuronal wiring diagram and amenability to a vast array of genetic and molecular tools, such as RNA interference, microarray analysis, and fluorescent probes [3,4].

Additional studies utilized fs-laser nanoaxotomy to begin discovering genes related to axonal regeneration in *C. elegans* [5,6,7]. Though this technique is becoming an established tool for *C. elegans* neurobiologists, to date no one has used it for genome-wide studies on the genetic and molecular basis of neural regeneration. One would need

to perform axotomies and imaging on hundreds or thousands of worms on the time-scale of days to make such studies practical.

With the considerable time and resources needed for genome-wide nerve regeneration studies in mind, we can turn to emerging biotechnologies to provide innovations to meet these challenges. Specifically, application of microfluidic engineering has yielded several new high-throughput biological assays. Recent advances in microfabrication techniques vastly improved the speed, flexibility, and applicability of electronic devices by reducing the size and cost of complex electronic circuits. Microfluidics exploits these methods to make systems of microchannels that reduce the scale, cost, and processing time of manipulating chemical and biological samples. Several research groups mainly led by Quake *et al*. have made microfluidic devices consisting of intricate arrays of pressure-controlled valves for multiplexed chemical and visual analysis of biological samples [8]. In the studies presented here, we developed and tested microfluidic devices for the immobilization, axotomy, and imaging of multiple *C. elegans* worms; a major step towards high-throughput nerve regeneration studies.

First, we used a device established for imaging and axotomy of mechanosensory neurons to investigate regeneration of motor neurons, which differ from mechanosensory neurons in morphology and location in the worm's body [9,10]. This device is a two-layered microfluidic chip that immobilizes worms with a ~25 μm thick deformable membrane (Figure 1). Motor neuron axons were cut and could regenerate in this platform with greater frequency and shorter duration than axons cut in animals that were immobilized with anesthetics on agar pads [2].

Next, we fabricated a simple, single-layer device that consisted of an array of microfluidic channels in parallel, which was capable of simultaneously loading and trapping multiple worms on-chip in a matter of seconds. This single-layer parallel trap device has several channels that taper to a width that prevents animals from passing through. As worms plug these channels, their bodies also significantly slow the incoming flow, diverting other inward bound worms into unfilled traps. This simple-to-use device can effectively immobilize the worms in a matter of seconds with nearly all of its traps filled. However, forcing the animals into thin channels deformed the worms' bodies such that optical access to neurons for laser axotomy and imaging was inadequate. The lateral sides of the worm's body are pressed against the sides of the microfluidic channels instead of the coverglass, making it difficult to image or perform laser surgery on the mechanosensory neurons.

In our next iteration of this device concept, we developed the first membrane immobilization parallel trap device. In this platform we improved optical access to the axons by trapping the worms in wider channels placed under downward deflecting immobilization membranes similar to that of the device in Figure 1. These wide channels were upstream of tapering channels, which would do the initial trapping before immobilization for imaging and laser nanoaxotomy. While it was now easier to cut axons, we encountered two main problems with this design. First, during the initial animal loading step, worms in the fluidic traps could not completely plug the tapering channels and prevent the incoming flow from bringing in additional worms into the same trap. Second, the new trapping channel geometries were still not wide enough to allow

sufficient deformation of the immobilization membrane to consistently stop worms from moving during imaging and laser axotomy. The membrane thickness also may have played a role in the membrane deformation malfunction.

We addressed the weaknesses of the first membrane immobilization parallel trap device in a third design. We widened the trap to facilitate membrane deformation during immobilization, and reverted the tapering channel geometry back to the specifications of the single-layer device. We also integrated a liquid nutrient perfusion channel that ran across the entire trap array to improve on-chip animal viability. The wider traps immobilized the worms completely with far less applied pressure than previous designs and allowed us to perform preliminary nerve regeneration studies on the oxygen-sensing neuron, PQR. However, the addition of the perfusion channel created a path for fluid flow into the traps, which already had worms stuck in their tapering channels, allowing multiple worms to enter single traps.

We finally propose a design that attempts to integrate the positive outcomes of testing these devices into a single platform. It will have an array of multiple traps arranged in parallel with respect to incoming fluid flow. The traps will consist of two main sections: a thin channel to initially trap the worm and a large area channel for immobilization. In this design, the thin trapping channel will be upstream of the immobilization channel and the immobilization membrane will be deflected downward during animal loading to prevent worms from over-filling the traps. These modifications will hopefully overcome the pitfalls of previous designs

Chapter 2: Motivation and Background

2.1 Motivation

2.1.1 Significance of Studying Nerve Degeneration and Regeneration

Neurodegenerative disorders, such as Alzheimer's, Parkinson's, and Huntington's disease affect nearly 5 million people across the United States. Understanding the physical, molecular, and genetic mechanisms behind nerve regeneration and degeneration could lead to the development of new therapies to tackle these ailments [1]. These phenomena can be studied in detail by severing individual nerve axons of model organisms under controlled micro-conditions and observing their subsequent behavior and regenerative characteristics. Additionally, precisely severing individual axons *in vivo* could serve as a tool to understand the neural basis of certain behaviors in these organisms. Scientists could discover the role individual neural connections (synapses between dendrites and axons) in a given nervous system circuit by deducing which neurons are essential to the system's function and seeing how axotomy and regeneration affect the loss and recovery of the circuit's behavior, respectively [11].

2.1.2 *C. elegans* Potential in Nerve Regeneration Studies

Until recently, *in vivo* studies of nerve regeneration after artificial axotomy have been limited to more complex organisms, such as mouse or zebrafish due to a lack of precise surgical techniques [3,4]. However, if the axotomy method could be scaled for simpler microscopic organisms, the fundamental biology of nerve regeneration

mechanisms would be more accessible. For example, the microscopic nematode *C. elegans* is one of the most versatile and widely used model organisms for experimental neurobiology. Scientists have characterized the function, anatomy, and connectivity of almost all of the 302 neurons in an adult *C. elegans* hermaphrodite [12]. Additionally, *C. elegans* was the first multi-cellular organism to have a completely sequenced genome, which shares extensive homology with higher organisms, even mammals.

Anatomical simplicity and a wide variety of genetic tools make *C. elegans* a very powerful model organism for studies of nerve regeneration and degeneration, *in vivo*. Recently, a mutant *C. elegans* strain was found that had hypersensitivity to RNAi gene knock-down in neurons. Researchers were able to screen across nearly 5,000 genes to find mediators of axon guidance and identified ninety-three gene candidates associated with axon defects [13]. Rapid manipulation and visualization of nerve regeneration in this simple organism will generate vast biological datasets that could be used to identify potential genetic drug targets for the treatment of neurological disorders.

2.2 Background

2.2.1 Femtosecond Pulse Laser Axotomy Studies in *C. elegans*

Our original studies in *C. elegans* focused on nerve regeneration of the D-type (DD, VD) motor neurons in worms whose axons were cut at the L4 life-stage [2]. We found that over 50% of the worms' axons completely reconnected to the distal portion of the neuron. Additionally, animals that had originally lost the ability to traverse backwards

(tail first) right after the axon cuts, regained full mobility when their DD and VD motor neurons reconnected to a segment of the neuron that was distal to the original cut site.

Since then, other groups have utilized the laser nanoaxotomy techniques developed in that initial study to investigate other aspects of neural regeneration in *C. elegans*. Wu et al. found that the mechanosensory neuron, PLM, regrew and reconnected with far fewer anterior-posterior guidance errors when laser axotomy was performed in early larval stage *C. elegans*, as opposed to late larval and adult animals [5]. They also found that the VAB-1 Ephrin Tyrosine Kinase receptor may play a role in these guidance errors in adults. Gabel et al. demonstrated that proper axon guidance during regeneration was dependent upon the cytoplasmic protein MIG-10/Lamellipodin and regulators of actin cytoskeleton formation; UNC-34/Ena and CED-10/Rac [7]. In two more studies, the DLK-1 Map Kinase pathway was found to be directly involved in the development and proper regeneration following axotomy in both motor and mechanosensory neurons in *C. elegans* [6,14]. Over-activity of this pathway leads to overgrowth of axons and synapse morphology defects, while axons cut with a fs-laser could not regrow as efficiently as wild-type animals if one of the genes in the pathway was missing.

For these studies, worms were individually hand-picked one at a time and transferred to agar pads with anesthetics (e.g. phenoxypropanol or levamasole) before being mounted on a microscope for imaging and axotomy. In addition to the toxicity of long-term exposure to anesthetics, this time consuming method would be prohibitive to large genome-wide investigations of nerve regeneration mechanisms in *C. elegans*.

The impetus for the work presented here was to develop tools to automate animal sorting, imaging, and targeted axotomy in *C. elegans*.

2.2.2 Microfluidics for Immobilization of *C. elegans*

Our lab recently applied recent advances in multi-layer PDMS (polydimethylsiloxane) microfluidic device fabrication to engineer a platform to study *C. elegans* worms at different phases between fs-laser nanoaxotomy and nerve regeneration imaging with conventional microscopy techniques [10].

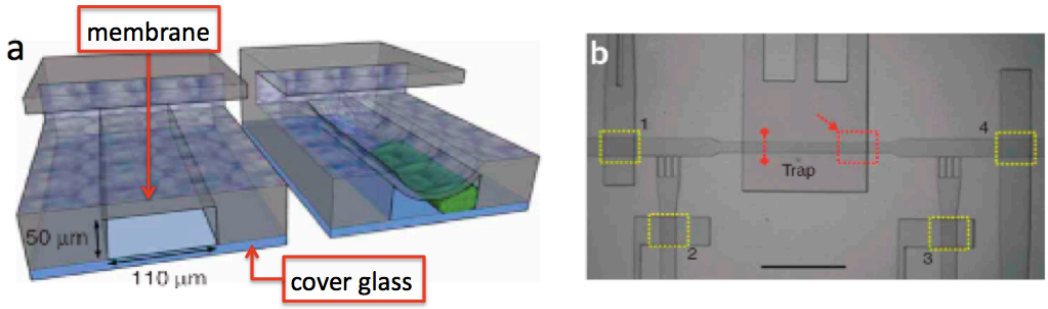

Figure 1: Microfluidic Lab-on-a-Chip for Imaging and Laser Nanoaxotomy of *C. elegans*. (a) Conceptual three-dimensional section renderings of the bilayer trap channels without fand with a worm (green) immobilized by a membrane. **(b)** View of the trapping system: Valves 1–4 (yellow rectangles) respectively control inlet regulation (1), fine positioning of the worm (2 and 3) and gating to the recovery chambers (4) (SCALE BAR ~1 mm). [10]

As shown in Figure 1, we designed and fabricated a lab-on-chip platform in which single animals were loaded into a microfluidic channel either manually or with a syringe pump before entering the microfluidic immobilization trap, which was essentially a deformable membrane above the channel housing the worm [10]. When we wished to image or ablate axons, pressure was applied to the channel leading to the membrane. The

membrane pressed the worm's body against the cover slip, which was bonded to the bottom of the device (Figure 1a). This orientation provided ideal optical access to neurons of interest. Off-chip controls were a set of computer-controlled solenoid valves and a syringe pump, which allowed automated control of fluid flow in the micro-channels. Another group at MIT subsequently developed a similar device for performing fs-laser axotomy and two-photon imaging studies of nerve regeneration in *C. elegans* [15].

With our membrane immobilization device, our lab studied nerve regeneration in *C. elegans* mechanosensory neurons (ALM, anterior lateral microtubule cell and PLM, posterior lateral microtubule cell) and we found that axonal recovery time was greatly reduced (~60-90 minutes versus ~6-12 hours) when compared to experiments performed on agar with anesthetics [10]. These studies demonstrated the feasibility of performing laser axotomy on worms in a microfluidic device, while suggesting that the animals' regeneration capacity was more rapid in the absence of anesthetics.

This device established the necessary components to immobilize, image, and perform laser nanoaxtomy: a fluid channel with the proper dimensions to house a single worm and a deflectable membrane to precisely immobilize the animal for optical studies [10]. The subsequent design question was how could these functional pieces be integrated into a high-throughput system that would enable the study of multiple animals (10's to 1000's) in a short period of time.

One solution to enabling high-throughput studies is serial automation. Precisely timed actuation of off-chip solenoid valves to activate on-chip membrane valves could

control the transport of worms in a microfluidic channel such that a large numbers could be sequentially studied with the afore-mentioned optical methods. This "one-by-one" approach requires only one imaging and surgery staging area to receive single worms, which are subsequently transported to another location on-chip or to an external storage platform as the next worm arrives for imaging and surgery. Chung *et al*. developed a microfluidic device that had one imaging channel receiving a single worm for imaging every few seconds [16]. Relying on this automated serial method to handle worms one-by-one, the researchers claim that the device sorted hundreds of worms per hour based on relative fluorescence intensity of certain cells in the worm's body [16]. One drawback for axotomy studies is that after surgery, the animals need to be moved to separate storage areas and then brought back to the imaging channel after a given amount of time to observe regeneration. Automation of this kind of process could become very complex if one wished to study the animals in large quantities.

Another route to high-throughput studies of *C. elegans* worms on-chip is parallelization. In this approach the number of channels for immobilization, imaging, and surgery would be increased by one or more orders of magnitude in the device design and arranged in a parallel fluidic circuit. This way one could simultaneously load and house many worms in their own individual imaging and surgery chambers in a single chip. An advantage of parallelization versus the one-by-one approach is that with the proper design, the complexity of automation and time spent sorting and transporting animals through the device is greatly reduced. Additionally, the worms can remain housed in their imaging and surgery chambers indefinitely between observations. Housing the worms in

parallel avoids repeatedly moving single worms out of the imaging and surgery portion of the chip for high-volume experiments. The primary disadvantage of this approach is that in order to study 100's or 1000's of worms one would need a large-area chip (several centimeters in diameter) or multiple chips to store the worms. Fabrication of large area microfluidic devices with two channel layers requires precise alignment of the valve control layer with respect to the fluid channel layer. Additionally, high-throughput studies would necessitate a motorized translation stage for optical observations of multiple chambers. However, this equipment is readily available for many standard optical setups.

A few groups have recently introduced simple microfluidic devices that utilize parallelization in their designs. A device made by Hulme *et al*. has a single inlet, which bifurcates seven times in order to create 2^7 (128) trapping channels that taper in width over a length of 5 mm from 100 microns to 10 microns [17]. Single animals get stuck in one of these tapering regions and block most of the flow through that particular channel, such that the likely-hood of another worm coming to that location is much lower than it following the upstream bifurcations to another open trapping channel. While the bifurcations limit worms from over-filling single channels, they necessitate a 15-20 minute loading time to fill the traps. Allen *et al*. developed a chip that consists of an array of tapering trapping channels in parallel placed downstream of a worm-loading inlet channel [18]. These five millimeter long trapping channels are 100 microns wide at their entrance and 8 microns at their opposite end, which is a small enough width to prevent the animals from squeezing through. A drawback to such long trapping channels is that

multiple worms may fill a single channel, which may create confusion in tracking individual specimens across multiple time points. Additionally, both devices mentioned in this paragraph require constant applied pressure to the inlet channel to guarantee long-term immobilization of animals.

We developed three new devices that operate on the parallelization design concept to make axotomy studies with *C. elegans* more efficient in terms of time and effort. We eventually came to the conclusion to use tapering channels arranged in parallel to initially trap worms, but to then house the worms upstream in wider channels for long term storage and immobilization via pressurized membranes above these channels.

2.2.3 Femtosecond Laser Ablation Physics

Femtosecond laser pulses have been suggested as a precise ablation tool for living tissue owing to their high peak intensities and ability to generate plasma locally and efficiently, while still operating at low laser energies (nanojoule range). Previous neural ablation studies in *C. elegans* used nanosecond pulse ultraviolet lasers, which require microjoule energies to cause ablation and lack the sub-cellular precision seen with fs-lasers [19]. The higher energy pulse lasers caused much more collateral damage to nearby tissue through thermal and mechanical processes. Alternatively, the ultra-short pulse durations and high photon flux of tightly focused fs-laser light are absorbed through non-linear processes, which result in very little damage to tissues outside of the focal volume.

Femtosecond laser ablation initiates through the absorption of photons in a condensed material (water, biological tissue, glass, etc.) followed by the freeing of

electrons through multi-photon, tunneling, and avalanche ionization. Exponential growth of free electrons beyond the critical density leads to the generation of a high-density plasma within the confined focal volume [20]. This plasma expands radially, emitting a shockwave that causes damage in the form of high shear stress. The plasma becomes a cavitation bubble, which expands until the internal pressure can no longer resist surrounding water pressure and collapses. However, the gas generated can expand again due to fast confinement to a small volume, recreating the bubble.

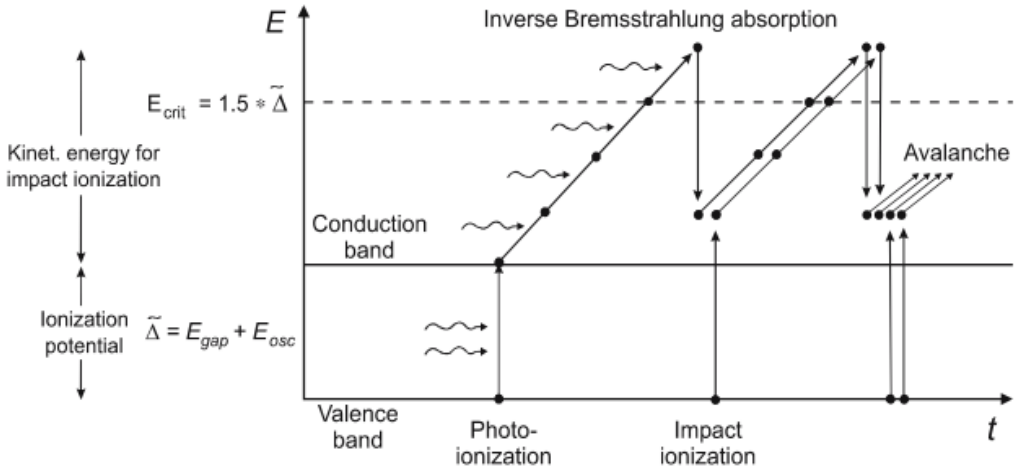

Figure 2: Absorption and Ionization Events that Lead to Ablation of Tissue. The roles of different photoionization processes, such as multiphoton absorption, inverse Bremsstrahlung absorption, and impact ionization in free electron formation at the focal volume of the laser during nanoaxotomy [20].

Briefly, the ionization events that lead to optical breakdown and photo-damage occur as follows (Figure 2). At the atomic level of the ablated material, multi-photon absorption by the electrons in the valence band excite these electrons to the higher-energy conduction band. After the electrons reach this state, several single photon absorption

events in succession raise the elections to an even higher energy state in a process known as ‘inverse Bremmstrahlung’ absorption. Then, one of these high-energy electrons collides with a conduction band electron with enough kinetic energy to excite it up to the valence band; a phenomenon known as impact ionization. The original colliding electron still keeps enough energy remain in the conduction band. Each time this cycle repeats, impact ionization doubles the number of electrons in the conduction band. After several cycles these events create an “avalanche” of free electrons in the focal volume that outnumbers the free electron loss through diffusion and recombination. The energy generated by this process must also outweigh energy loss due to photon-to-large particle collisions that are asynchronous with photon absorption. When a critical density of electrons is freed at the focal spot, optical breakdown causes physical damage to the material [20].

2.2.4 Fluid Dynamic Modeling

The development of microfluidic chips relies heavily on intuition and experience from testing and modifying the devices in conjunction with mathematical approaches from fluid mechanics. The intuitive approach is used to develop the basic conceptual chip design, while mathematical methods help optimize fluid flow profiles and flow rates.

The process of calculating the essential fluid flow characteristics for microfluidic systems can be accomplished by reducing the system to a fluidic circuit, as illustrated in Figure 3 [21]. The bulk fluidic resistances of the major components are then calculated

based on their geometries, followed by the pressure drop across each component. One can designate a given injection pressure from the fluid source based pressures used experimentally and assume that the gauge pressure at the outlet is zero (atmospheric pressure). Once they find the pressure coming into the chip inlet, they can enter these parameters into a computational model to obtain fluid profiles and velocities within a given microfluidic design.

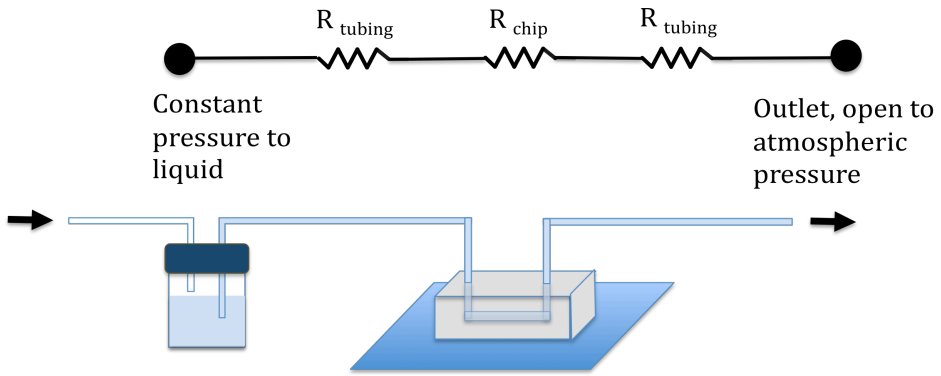

Figure 3: Fluidic Circuit Model. Here is a basic fluidic circuit model of a microfluidic system with flow driven by a constant pressure source. R_{tubing} is the fluidic resistance of the tubing either before or after the chip and R_{chip} is the overall fluidic resistance of the microfluidic device. A fluid source under constant gauge pressure (known) is fed to the chip from tubing and then exits the chip through additional tubing to atmospheric pressure.

2.2.5 The D-type Motor Neurons

In each fully developed worm, there are 19 commissural DD (dorsal D-type) and VD (ventral) motor neurons and 16 of them can be cut without killing the animal based on our previous experiments [2]. These GABA-ergic neurons innervate the body wall muscle cells and extend from the dorsal cord to the ventral cord [9]. As illustrated in Figure 4, we cut the motor neuron axons mid-way between the primary nerve cords.

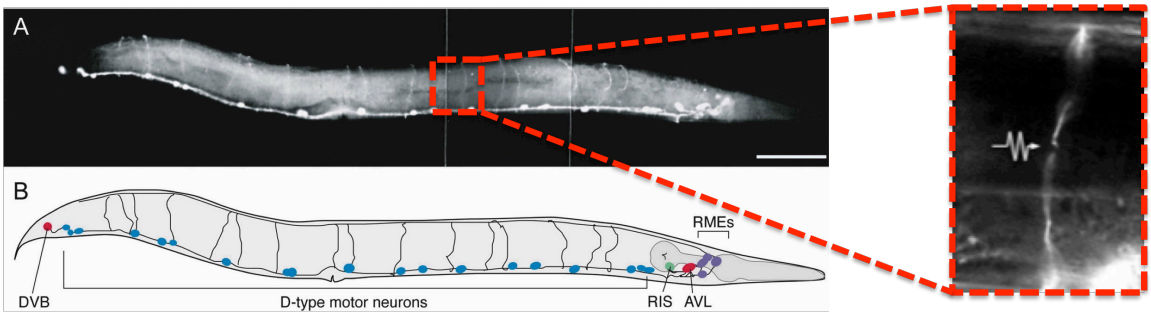

Figure 4: D-type motor neurons. (a) Fluorescence micrograph of all GABA containing cells, including the D-type motor neurons, which were severed midway between the ventral and dorsal cords for these studies. This is an adult hermaphrodite. (SCALE BAR ~100 µm) **(b)** Schematic showing the locations of the D-type DD and VD motor neurons along the animal's body labeled blue. (note: Figures 5A and B, excluding the axotomy image were adapted from [9])

We tested the regenerative capacity of these neurons in L4 worms on the microfluidic platform originally developed by Guo et al. [10]. These studies confirmed that the microfluidic membrane immobilization method provided enough optical access for imaging and fs-laser nanoaxotomy of the motor neurons.

2.2.6 PQR Oxygen-Sensing Neuron

This PQR neuron's cell body is located near the tail and extends out neural processes in two directions (Figure 5). The short process or "dendrite" extends out towards the tail and has no synapses or gap junctions, while the ventral cord process or "axon" extends toward the head along the ventral cord where it has multiple synapses. The primary purpose of this neuron is oxygen sensation inside the animal's coelomic body fluid cavity [22]. We performed preliminary axotomy studies with the membrane

immobilization parallel trap device #2 on the regenerative capacity of this neuron. We wanted to see if there was a difference in regeneration frequency and duration between the dendrite and the axon. Imaging and axotomies were performed on the second membrane immobilization device proposed in chapter 4

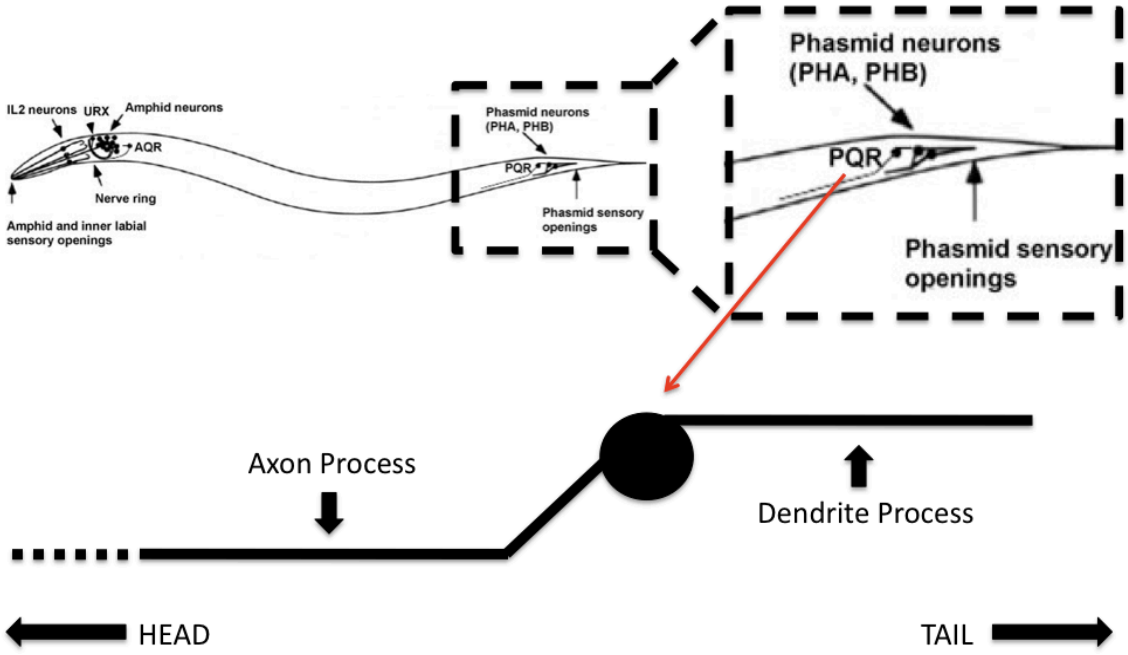

Figure 5: Anatomy of the PQR Neuron. This oxygen sensory neuron is located in the left lumbar ganglion on the posterior-lateral side of the body, and has two processes emerging from the cell body: a dendrite extending posterior toward the tip of the tail and an axon extending anterior joining the ventral nerve cord (the dotted line indicates that the axon continues towards the head for ~100-200 µm) [23].

.

Chapter 3: Experimental Methods and Tools

In this chapter we outline the tools and experimental methods used to perform the various studies that are described in this thesis. We used standard *C. elegans* biology techniques for our worm studies. For microfluidic chip fabrication, established soft-lithography methods were utilized. Finally, femtosecond pulse lasers were coupled to our home-made optical set-up to perform nanoaxotomy on the worms in our microfluidic platforms.

3.1 *C. elegans* Culturing

C. elegans worms were grown on NGM (nematode growth medium) agar pads seeded with OP50 *E. coli* bacteria lawns at 20º C. Age-synchronous populations were maintained by bleaching adult worms and isolating their eggs, which are then transferred to a fresh agar pad with bacteria. After roughly 42 hrs the worms reach the L4 larval stage and are used in the axotomy studies.

3.2 *C. elegans* Strains

In order to study the regenerative capacity of the D-type motor neurons we used the C. elegans strain, *juIs76* [Punc-25::GFP], which visualizes the D-type ventral cord motor neurons with GFP (green fluorescent protein). For the PQR neuron regeneration studies, we used the strain *kyIs417* [Pgcy-36::GFP, odr-1::RFP], which visualizes the PQR, AQR, and URX oxygen-sensing neurons. For mechanosensory neurons, the strain

zdIs5 [Pmec-4::GFP] was used, which expresses GFP in the ALM, PLM, ALN, AVN, and PVN neurons.

3.3 Optical Axotomy Set-up

Figure 6 presents the optical setup used for axotomy studies. The laser beam is tightly focused on the target through an oil-immersion high numerical aperture objective lens (Zeiss 63x, NA=1.4). The fluorescence imaging system consists of a mercury lamp and a FITC filter set. The excitation filter and the emission filter transmit wavelength ranges of 460-500 nm and 510-560 nm, respectively. The dichroic mirror reflects wavelengths smaller than 510 nm. A cold mirror is used to transmit the laser beam but reflect the fluorescence emission towards a CCD camera (Princeton Instruments, "Cool-Snap") for epifluorescence imaging. The resulting emission from the focal plane is collected by the tube lens and detected by the CCD camera. A filter blocks the scattered laser light. In our case the sample could be worms immobilized on agar and anesthetics or a microfluidic device loaded with worms.

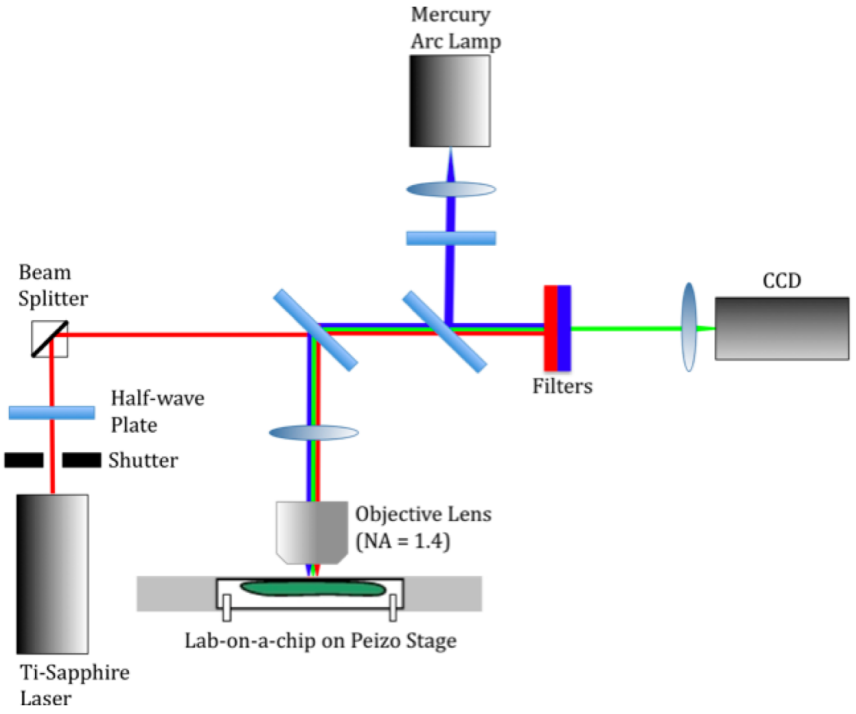

Figure 6: Optical Setup. A schematic of the optical setup for imaging (optical, fluorescence, and two photon imaging modalities), and femtosecond laser nano-surgery in *C. elegans*.

Femtosecond laser pulses were created by a regenerative amplifier (Spectra Physics, "Spitfire") seeded by a Ti-Sapphire mode-locked laser (Spectra Physics, "Tsunami"). The system generates 1 mJ energy, 220 fs short pulses at a 1 kHz repetition rate (Figure 7). For most of our experiments, we delivered a single burst of 200 pulses to the focal volume using the precisely timed mechanical shutter. The laser energy in the specimen can be precisely varied with a half-wave plate that rotates the polarization of the laser beam and a cube beam splitter, where the intensity of the transmitted light depends on its polarization. A fast mechanical shutter is used to select the desired number of pulses for the ablation experiments.

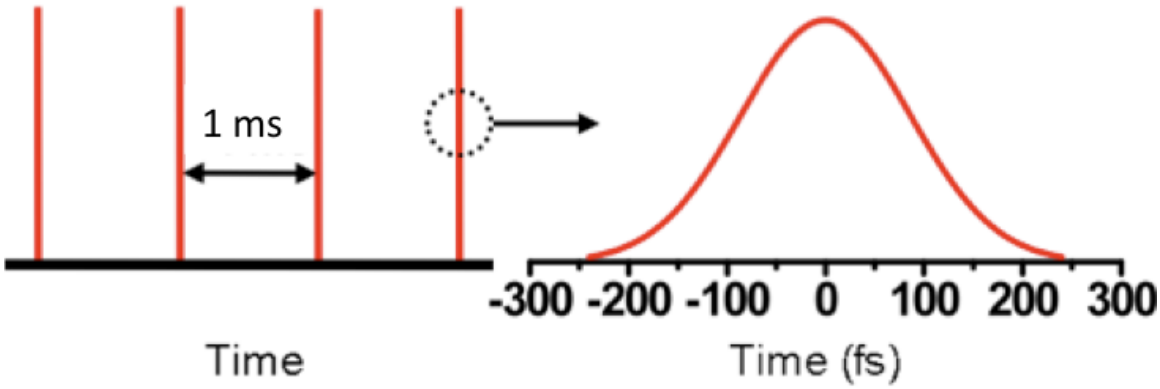

Figure 7: Femtosecond Laser Pulse Timing Characteristics. The surgery beam usually comprises of a train of 220-fs pulses spaced in time by 1 ms. The axotomy is performed with 200 pulses with an energy per pulse of 7.2 to 10 nJ at the ablated tissue.

3.4 Axon Targeting for Fs-Laser Nanoaxotomy

Figure 8 illustrates the general procedure of targeting and cutting an axon followed by the observation of subsequent reconnection. In this case we used the *zdIs5* strain and cut one of the two ALM mechanosensory neurons, which are located at the right and left lateral mid-bodies and extend their axons to the head. The apparent cut shown in Figure 8b results in the outgrowth of the axon stump proximal to the neuron cell body (to the right) towards the distal axon stump 12 hours later (Figure 8c). In this case the proximal axon passes a few microns to left of the axotomy site when it connects to the distal axon. There is much observed variation in the morphology of these regeneration events across different animals. This variation includes the proximal end not regrowing, proximal end regrowth without actual reconnection to the distal end (which leads to excessive branching of the proximal end), and reconnection of the proximal end to various spots along the distal fragment.

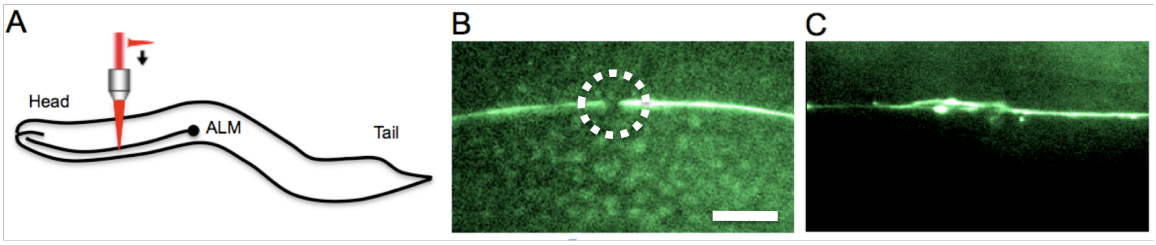

Figure 8: Laser Axotomy of ALM Mechanosensory Neuron Followed by Axonal Reconnection on Agar. (a) Delivering laser pulses to an ALM mechanosensory neuron in an L4 stage worm. **(b)** GFP labeled axon of the ALM neuron immediately after axotomy. (SCALE BAR ~5 µm) **(c)** Reconnection of the axon in (b) from the end proximal to the ALM cell body (right) back to its distal partner (left) 12 hrs post-axotomy.

3.5 Fluid Dynamic Modeling of Flows in Microfluidic Chips

our calculations indicated that the microfluidic device had a laminar flow due the low Reynold's number:

$$\mathrm{Re} = \frac{d\rho u}{\mu} \qquad (1)$$

Here d is the characteristic distance or diameter of the given tube, ρ is the density of the fluid, u is the fluid velocity, and µ is the viscosity. Low Reynold's numbers are generally expected at microfluidic length scales, and laminar flows tend to dominate [24]. We calculated Reynold's numbers in the range of 0.1 for our microfluidic trapping channels, which is *well* into the range for laminar flow (these were based on a 100 micron wide channel with a mean fluid velocity of 1 mm/sec filled with water).

For the tubing connections, which externally interface into the microfluidic chips, the fluidic resistance can be estimated from the characteristic equations describing a fully developed laminar flow of Newtonian fluid in a circular tube:

$$R = \frac{128\mu L}{\pi d^4} \tag{2}$$

Here, L is the length of the tube and d is the diameter of the tube. The $1/d^4$ dependence of resistance on diameter makes even single order of magnitude differences in diameter lead to vast changes in resistance.

Fluidic resistance across the microfluidic channel is determined by another method because microfluidic channels have rectangular cross-sections with dimensions on the order of tens of microns. In order to get an analytical solution to the fluidic resistance of the micro-channels, we used a solution of the Navier-Stokes equations for an isothermal, incompressible, isotropic liquid flow with no slip boundary conditions at the rectangular side-walls. Below is the final expression to estimate microfluidic resistance in a rectangular cross-section channel, which was described in [25]:

$$R = \frac{128\mu L}{wh^3}\left[1 - \frac{h}{w}\left(\frac{192}{\pi^5}\sum_{n=1,3,5}^{\infty}\frac{1}{n^5}\tanh\right)\right]^{-1} \tag{3}$$

Here, w is the smaller dimension between the width and height of the rectangular channel, while h is the larger dimension. All other variables are identical to their

definitions in equation 1. Based on our calculations resistance of the tubing coming into the chip was less than 0.1 % of the resistance of the entire chip, due in part to the large difference in L between the microfluidic channel (1 mm) versus the tubing (10 cm).

With the characteristic flow rate of the system, we can next calculate the pressure drop after each resistance in the system and then use this information to perform computational rendering of flow profiles in the actual microfluidic devices. These parameters are related to each other by the simple fluidic circuit model, where ΔP is the pressure drop, Q is the volumetric flow rate, and R is the fluidic resistance across a particular channel:

$$\Delta P = QR \tag{4}$$

We modeled the microfluidic flow profile in the finite element multiphysics software, COMSOL. Under specific physical conditions, we can take a microfluidic chip design and apply different boundary conditions for flow rate, pressure, and viscosity throughout the layout of the chip design. The software will numerically calculate the chosen parameters until it reaches steady state.

COMSOL has a module geared toward modeling MEMS (micro-electromechanical systems), which has a sub-module for microfluidic flow governed by the Navier-Stokes equations for incompressible flow under steady state:

$$\begin{aligned} &\nabla \bullet u = 0 \\ &-\nabla \bullet \mu(\nabla u + (\nabla u)^T) + \rho(u \bullet \nabla)u + \nabla p = 0 \end{aligned} \tag{5}$$

Here u is the flow velocity vector (m/s), μ is the viscosity, ρ is density, and p is

pressure. If the layout of the microfluidic channel design had any geometric symmetry, we only modeled the portion of the channel that repeated along the symmetry plane. Taking into account symmetry drastically improved computational efficiency and saved time.

3.6 Microfluidic Device Fabrication

Microfluidic devices are usually fabricated with a technique known as soft lithography. Typically, a pattern is defined in a photolithographic mask that will be used to generate a pattern in a photosensitive material (photoresist) that is spin-coated onto a silicon wafer surface. This pattern serves as the mold for an elastomer (PDMS) that is poured onto the wafer. Then, one hardens and removes the elastomer from the wafer and finally bonds the elastomer mold to a substrate, such as glass or silicon.

Two photoresist molds are needed to fabricate double-layer microfluidic devices with deformable membranes. For the bottom layer, which usually houses the *C. elegans* worms, PDMS elastomer is spin-coated across the mold so that a 20-30 μm layer rests above the photoresist features. This layer will serve as the membrane component of the microfluidic valves. After the PDMS has hardened, the top layer of the device, which is usually fabricated as its own single layer in the typical fashion mentioned earlier, is bonded to the bottom layer. Both layers are then removed as one piece, which has fluidic access holes drilled into it. The entire two-layer elastomer chip is then finally bonded to a microscope cover glass whose optical specifications are matched to the objective lens in our laser ablation system.

3.7 Microfluidic Device Operation

For experiments requiring us to load just fluid or fluid with animals in suspension into the microfluidic devices we used 22 guage fluidic couplers (Instech Laboraties Inc.) fitted to polyethylene tubing, which we then attached to fluid-filled syringes. In order to avoid the creation of bubbles inside the microchannels, the device was completely sealed with plugs at every fluid access hole except for one, which was used to deliver fluid for pre-loading. Since PDMS is permeable to gas but not liquid, fluid and bubbles initially delivered into the chip would pressurize and the all the bubbles would escape through the PDMS. The couplers have a slightly higher diameter than the holes punched into the micorfluidic chips, which ensures a liquid-tight seal when delivering fluid into the device.

Generally, worms were suspended in M-9 buffer solution by adding 1-2 mLs to the surface of an agar pad where the animals were being cultured. Then they were pulled up into a M-9 buffer-filled syringe via the coupler and polyethylene tubing by applying vacuum to the syringe. Finally, we fit the coupler into the fluid access hole of the chip and applied positive pressure to the syringe to deliver animals into the chip. Additional operational protocols specific to each of the three new devices are outlined in the following chapter.

Chapter 4: Novel Parallelized Microfluidic Devices for *C. elegans* Nerve Regeneration Studies

4.1 Overview of New Microfluidic Devices

In this chapter, we describe the design and testing of three iterations of the parallelized microfluidic device concept for trapping, housing, imaging, and axotomizing *C. elegans*. These devices were built to increase the number of axotomies and images one could acquire in a given amount of time by trapping many worms simultaneously for nerve regeneration studies. We present the devices in the chronological order of their development to demonstrate how we attempted to integrate knowledge from the each generation to improve overall functionality of subsequent designs. Key aspects of proper device operation were the percentage traps filled with worms, ability to immobilize worms for optical studies, and long term animal storage capability for observations at different time points. Other factors such as the rate of fabrication defects, long term animal viability (several days), and ease-of-use also played roles in evaluating device functionality.

All devices were fabricated using standard soft-lithography methods for the making of PDMS microdevices. Our first design was the single-layer parallel trap device, which established a method for delivering multiple worms in unison to individual traps, which were essentially channels that gradually tapered in width [17]. We then fabricated the first version of the membrane immobilization parallel trap device, which

circumvented the need pressurize worms in tapering channels for immobilization by housing worms beneath deformable membranes.

Finally, we made a second version of the membrane immobilization device, in which we improved the deformable membrane function by having even wider trapping channels. It was also outfitted with a nutrient perfusion channel to improve animal viability during long-term on-chip studies. Unfortunately, these perfusion channels had deleterious effects on parallel worm trapping efficiency, even if we plugged their tubing-to-chip inlets. However, we were still capable of performing preliminary nerve regeneration studies on the PQR neuron (oxygen-sensing) with relative ease on this design. Overall, each device had a number of advantages and disadvantages as a platform for efficient trapping of multiple worms, long-term animal storage, and high-throughput imaging and nanosurgery. The development of these devices will eventually lead to the optimization of the next generation of high-throughput microfluidic *C. elegans* nanoaxotomy platforms.

4.2 Design #1: Microfluidic Single-Layer Parallel Trap Device

The microfluidic single-layer parallel trap device was meant to be a simple-to-use platform for simultaneous immobilization of multiple *C. elegans* worms for easier imaging and laser nanoaxotomy. Our goal was to create a device that did not necessitate membrane valves and superfluous liquid inputs. This device only required three external liquid interfaces for proper function. The platform had 24 trap channels arranged in parallel with respect to the incoming flow from a single inlet channel. The trapping

method for this device is similar to the one used in S.E. Hulme et al.'s chip [17]. Each trap channel housed a single worm that was stuck between the channel walls because the width between them decreases from 50 μm to 10 μm. Optical access for microscopy and laser-axotomy was provided by the cover glass bonded to bottom of the device.

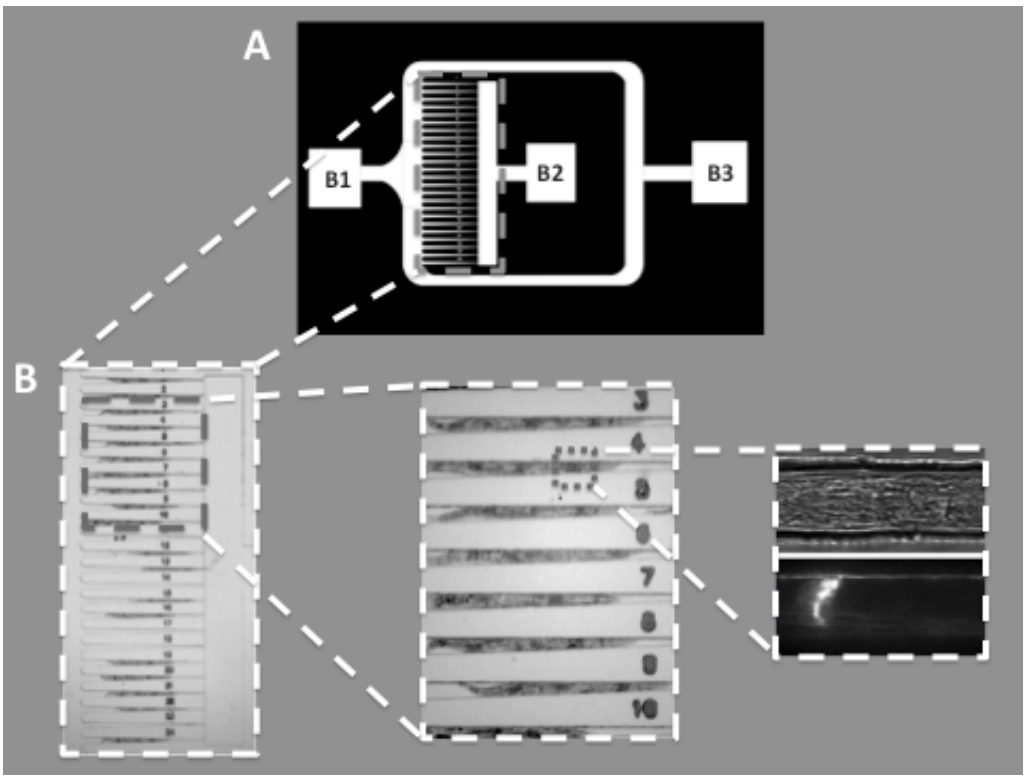

Figure 9: Design #1: Single-Layer Microfluidic Trap Array. (a) Schematic: Worms enter through B1 via injection from syringe-pressurized tubing coupled to the chip. A pressure gradient is created only between B1 and B2 so that worms will fill the tapering trapping channels (24 total). After a single worm is in each trap, flow into B3 is open to atmospheric pressure to wash out any excess worms that have accumulated in non-trap areas. **(b)** Worms fill almost all of the chip's trapping channels for imaging and laser axotomies.

Figure 9 shows the schematic and basic function of the single layer microfluidic device. There were three interfaces (B1, B2, B3) for fluidic access to the chip. Pressure gradients could be generated across the chip between two or three of the fluidic interfaces with a syringe (by hand or syringe pump) or with constant pneumatic pressure applied to a fluid source coupled to the chip. B1 was the primary entrance for worms to enter the chip, after which the animals entered one of the twenty-four trapping channels or exited the chip entirely by bypassing the traps and going to B3. Flow to the principle outlet (B3) was stopped by closing off an externally connected syringe valve, directing all of the flow to the twenty-four tapering trap channels, where worms were immobilized. At a length of 1200 μm, the tapering trap channels were 50 μm wide at their entrance and reduced down to a width of 10 μm at a linear rate. The dimensions of each trapping channel were meant to accommodate only one worm in the L4 development stage or larger. An L4 worm tends to be 600-700 μm in length on its anterior-posterior body axis and about 30 μm in diameter along its dorsal-ventral axis [26]. Additionally, the trapping channels were numbered for referencing animals between observations.

4.2.1 Design #1: Results

The device was demonstratively efficient at loading worms and filling the majority of the tapering channels in a short amount of time (less than a minute) when worms were loaded with a syringe manually. This is a major improvement over Hulme et al.'s bifurcating-channel device, which took roughly 15-20 minutes to fill most of its traps [17]. As long as pressure was applied to B1, the worms would remain in their traps

for observations and experiments. However, if this applied pressure to B1 was too high ($\geq$35 kPa), L4 worms could squeeze through the opposite ends of the trapping channels and exit the chip through B2.

Figure 10 illustrates the fluid dynamic simulations of this device during worm loading. In this model there is 2 psi gauge pressure (~14 kPa) applied to the imagined external fluid source and this flow goes directly to B1 and then the tapering worm traps, which are all open to atmospheric pressure (B2 is at 0 gauge pressure). In this case flow to B3 is completely blocked, acting as a dead end to fluid flow. We also blocked B3 during actual device tests of worm loading.

The flow velocity is relatively high as it enters at B1 and quickly dissipates by a factor of ~3 as it spreads across the large area of the entrance of the tapering trap channel array. The velocity then increases almost exponentially as the flow enters each trap because the hydraulic diameter of these tapering channels decreases at a linear rate along their length. Figure 10b shows fluid flow profiles across the trapping channels. The flow profile shows that the traps at the periphery of the array do not receive as much fluid flux as their counterparts at the center of the array, which are directly in front of B1. However, as the graph illustrates, the fluid velocities at the ends of the tapering channels are fairly uniform across the entire array (average velocity: 1280 mm/s $\pm$ 34). Tests with the actual device showed that the worms could fill almost all the traps, as long they had no blockage due to debris. We attribute the successful worm-loading into individual trap channels to the fact that the dimensions of the traps limited their capacity to one animal and flow to

filled traps in the center of the array is reduced to a degree that the unfilled traps on the periphery would subsequently receive most of the flow.

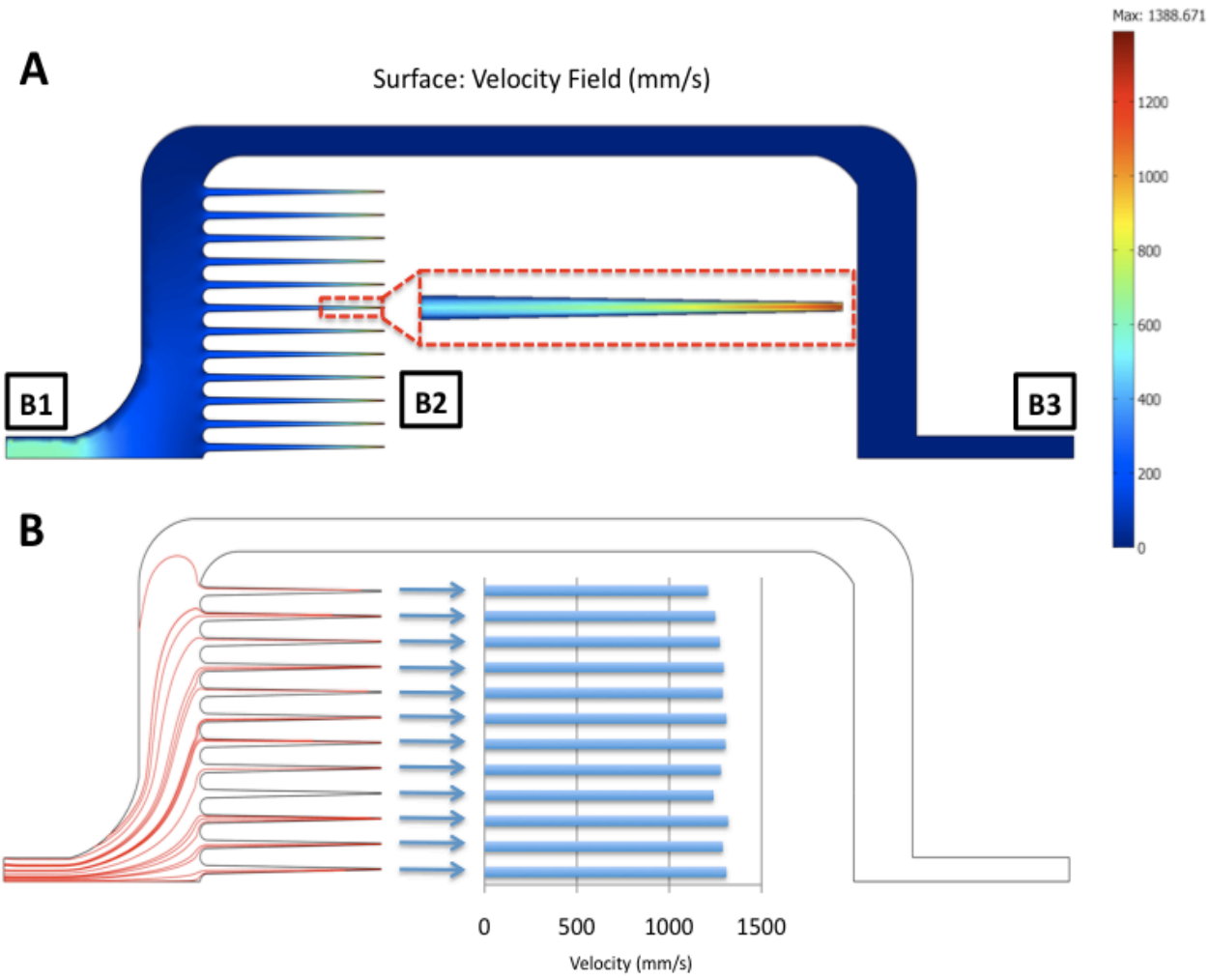

Figure 10: Fluid Dynamic Simulation of Single-Layer Parallel Trap Device. (a) COMSOL velocity field simulation, with the tip of a single tapering channel highlighted and labels showing the approximate location of the device's fluidic interfaces (B1, B2, & B3). **(b)** A flow profile simulation into the tapering trap channels, with corresponding fluid velocities at the channel tips (all values are exact for those particular tapering channels).

4.2.2 Design #1: Discussion

Like the previously described parallelized microfluidic traps for *C. elegans* [17,18], this device required constant applied pressure to maintain the worms in their trap channels for long-term observation. There was a concern that keeping the animals immobilized against the channel walls of the traps for a long period time could cause physical damage to their outer cuticle.

The main concern with this design, however, was in regard to imaging and targeting the axons for ablation. For our particular studies, the axons of the pertinent neurons (ALM, PLM, VD, DD, PQR) run along worm's lateral body-axis plane within microns from the outer cuticle; the outer surface of the worm's cylindrical body. Our laser nano-axotomy system was designed for animals with this body-axis plane parallel to the optical path, resulting in the axons being directly beneath the cover glass and the cuticle. This orientation allows for efficient delivery of photons to the axotomy site. However, in the single-layer parallel trap device, most worms stuck in a tapering channel would orient the lateral axis plane of its body perpendicularly to the optical path (Figure 11). Worm body orientation in the tapering channels requires that the laser beam focus pass through the cover glass and a significant portion of the worm's body to reach the axon, as opposed just glass and the worm's outer cuticle. Furthermore, these light scattering conditions caused low contrast imaging of axons (Figure 11a). When compared to optimal orientation, which was reproducibly achieved in Guo *et al.*'s device, the difference in imaging quality is clear (Figure 11b) [10]. Consequently, we were unable to

consistently produce visible axon cuts in this device with our high numerical aperture oil-immersion objective lens (Olympus 63x, NA=1.4).

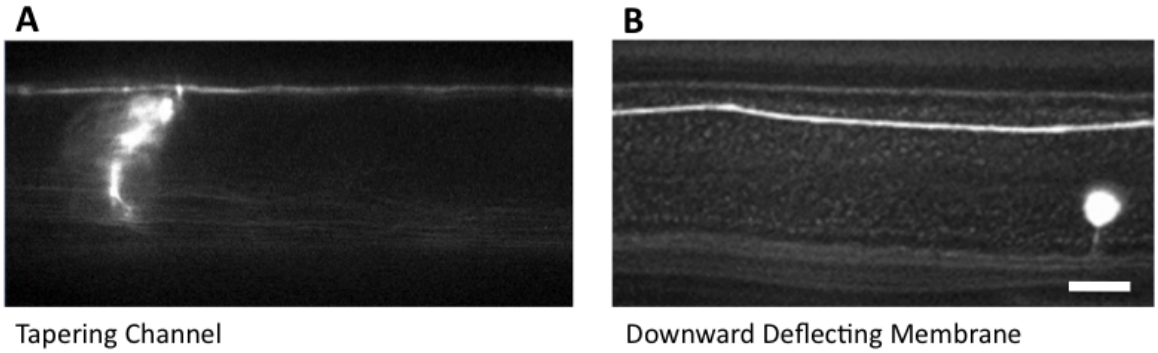

Figure 11: Optical Access Comparison for Two Microfluidic Devices. A comparison of optical access to axon using the tapering channel immobilization versus downward deflecting membrane from Guo *et al*.'s device [9]. **(a)** Poor optical access to ALM neuron due worm body orientation in the tapering channel device (design #1). **(b)** ALM neuron easily visualized during membrane immobilization of a *C. elegans* worm on Guo *et al*. 's chip. (SCALE BAR ~10 μm)

4.3 Design #2: Membrane Immobilization Parallel Trap Device (Version 1)

Next, we decided to pursue the new design shown in Figure 12, which would hopefully trap multiple worms in parallel, improve optical access to axons of interest, and allow for healthy long-term storage of the animals. First, for worm immobilization, we returned to the principles of our first published microfluidic device by integrating deformable membranes above regions that would house the animals [10]. In order to accomplish this, we changed the tapering channel traps into a wider rectangular channel (1000 μm x 100 μm), which was just downstream of a smaller tapering channel (200 μm in length). The rectangular section provided enough area for the membrane to deflect towards the animal for immobilization and allowed animals much more freedom of

movement between immobilization steps. We shortened the length of the tapering region of the trapping channel to keep the overall channel length short enough to discourage multiple worms from filling the traps. This tapering region was meant to trap worms initially in the same fashion as the single-layer parallel trap device. Finally, we placed another membrane valve in front of all of the immobilization chambers (T1 in Figure 12). This membrane valve prevents worms from escaping from traps' entrances, negating the need to keep the constant pressure on the worms for long-term storage on-chip.

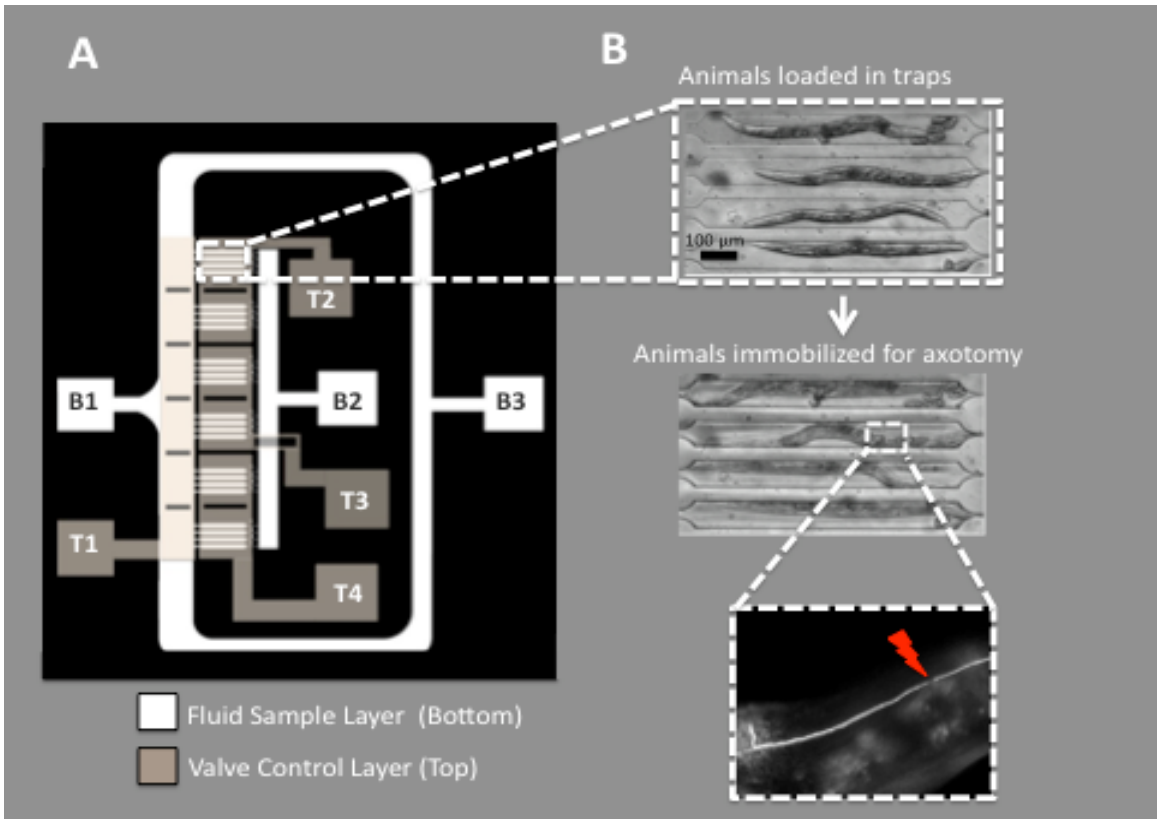

Figure 12: Design #2: Membrane Immobilization Parallel Trap Device (Version 1). (a) The fluid sample layer (white) accommodates worms and fluid flow and is bonded directly to a glass coverslip. The valve control layer (brown) is bonded to the previous elastomer layer from above in order to control fluid flow and animal immobilization. Worms enter through B1 via pressurized injection. Flow is only allowed to pass from B1 to B2 so that worms will fill traps (24 total). After all traps house at least one worm, T1 is pressurized to prevent worms from leaving their traps. Subsequent observations and axotomies can now be performed. **(b)** A single multi-trap section. Worms have filled individual traps. T2-T4 are then activated to depress the membranes across the worms' bodies for immobilization, which enables precise axotomy and imaging.

The device is composed of two stacked layers of microfluidic channels. The bottom layer (Figure 12, white channels) contains *C. elegans* animals in M-9 solution or growth medium, which are loaded through an inlet (B1). Excess fluid, bubbles, and animals can be flushed out through the channel opening (B3). This layer contains an

array of twenty-four traps for housing and immobilizing individual worms. These traps are arranged in groups of four and the dimensions of each trap are 1000 μm x 100 μm to accommodate L4 up to full adult growth stage worms. The animals can stay in these channels for several days if kept in nutrient media (CEHR), which eliminates the need to transfer them to agar plates between experimental steps, saving time and labor.

The worm loading steps are identical to the procedure used with the single layer parallel trap device. A pressure gradient must be generated from the inlet (B1) to the trap outlet (B2). Worms in solution are injected into the device via B1 during the simultaneous opening of outlet B2 to atmospheric pressure and complete occlusion of flow through B3. The individual traps taper in width right before outlet B2 such that worms will not escape and most of the flow will be blocked once a single worm has entered a trap (Figure 13, step 1). Much like the single layer parallel trap device, this blockage of flow by the worm's body in the tapering region is meant to minimize overfilling of a single trap with multiple worms.

Once the traps are filled with worms, we engage the second microfluidic channel layer (Valve Control Layer, brown) to immobilize the worms. First we pressurize T1 at (207-276 kPa) to activate the valve and block worms from exiting the trapping channels. The initial pressure applied to B1 for loading the animals is shut off and the pressure difference between B1 to B2 is allowed to equalize. The lack of a fluidic pressure gradient towards B2 causes the worms to move a several microns away from the tapering region, toward the trap entrance (Figure 13, step 2). In order to immobilize worms for precise imaging and axotomy, T2-T4 are also pressurized (207-276 kPa), which

downwardly deflects the appropriate membranes above the traps and presses the worms' bodies against the cover glass beneath the fluid sample layer (Figure 13, step 3). This body orientation gives better optical access to a given worm's axons for imaging and ablation.

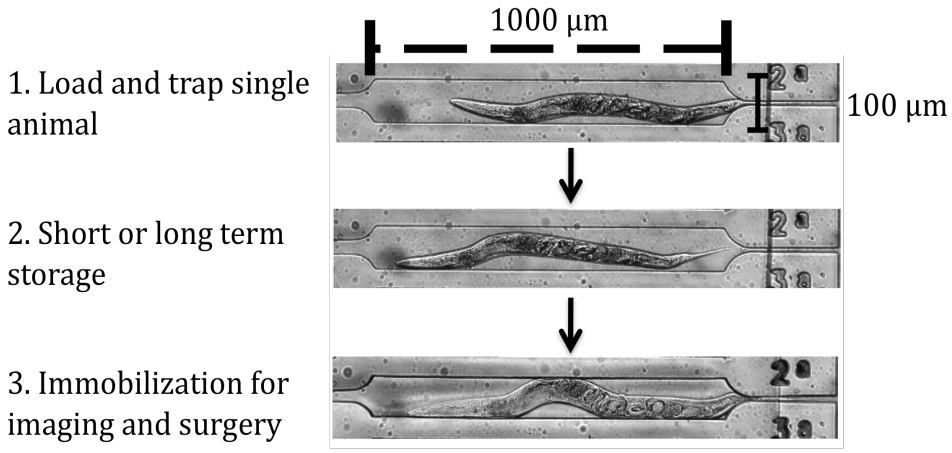

Figure 13: Design #2 Worm Immobilization. Steps of trapping of a single worm by the tapering channel during loading in the membrane immobilization parallel trap device (version 1).

4.3.1 Design #2: Results

The dimensions of the trapping channels in this device succeeded in providing a hospitable environment for long-term storage of worms over the course of an experiment. Nearly 100% of the animals survived on-chip for more than 24 hrs with proper nutrient media. For long-term storage, membrane valve T1 prevented worms from escaping their immobilization chambers as long as the valve remained pressurized over time. When worms were sufficiently immobilized, we were able to cut ALM axons and image adequately for nerve regeneration studies.

However, several tests of the device showed multiple worms moving to a single trap channel, while other traps remained empty. In many occasions, traps closer to the main inlet (B1) would fill with multiple animals, while traps at the top and bottom of the array would remain completely empty. This pattern of trap filling would suggest that the flow profile across the entrances of the trap array did not significantly favor peripheral traps once traps at the center were filled. If the trapping channel geometry did not allow the worms' bodies to adequately block flow in the tapering regions, then additional worms could go to filled traps at the center of the array. This would allow the traps to be overfilled, without diverting worms to peripheral traps.

When multiple animals were in a single trap, the membrane could not always downwardly deflect to the degree necessary to completely immobilize the worms for ablation and imaging.

4.3.2 Design #2: Discussion

Relative to Design #1, this second device allowed for much better imaging and ablation of axons in addition to the ability to keep animals alive for up to three days on-chip due to the larger dimensions of the trap channels. However, there was some efficiency lost in terms of loading the worms relative to the previous design.

Our main concern was its ability to fill all its traps with a single animal. It was expected that once a worm was stuck between the walls of the tapering channel of a given trap (Figure 13, Step 1), its body would plug the channel and the flow rate into that area

would decrease sufficiently so that no more animals would enter. However, the tapering channels had a rectangular cross-section and the animals' bodies were essentially cylindrical, making the complete occlusion of flow impossible. Though this was also been the case in Design #1, its trapping channels' dimensions only fit one worm at a time regardless of flow into the channel. Secondly, Design #1's tapering channel geometry allowed more surface area of the animals' bodies to plug flow. In fact, the more gradual tapering of the trapping channel in the single layer device could fit an entire worm's body (Figure 14, top). On the other hand, the tapering region of the Design #2 was much shorter and thinner, allowing only the head or tail to fill the tapering portion (Figure 14, bottom). Thus, worms blocked flow more efficiently in the tapering channels of the single layer device versus the membrane immobilization chip (version 1). Thus, we often saw multiple worms enter a given trap.

The presence of more than one worm sometimes prevented the immobilization membranes from adequately deforming and keeping worms immobilized. However, improper immobilization may have also been caused by larger membrane thickness due to improper soft-lithography fabrication. Unfortunately, when there is more than one animal in a single trap, long-term follow-up imaging of individual worms cannot be reliably accomplished without the possibility of losing track of specific animals in one trap at different observation time steps.

Also, the fact that the traps were not equidistant from the main inlet (B1) also may have contributed to the problematic animal trapping. The traps in the direct path of B1 seemed to receive more flow than traps towards the top and bottom of the trap array; a

result also seen in the flow simulations for design #1 (Figure 10), which had a very similar trapping channel array layout. Due to fact that the incoming flow to these center traps was not fully blocked by animals in the tapering regions and the size of the immobilization chambers accommodated multiple worms, flow of worms was less likely to be diverted to immobilization chambers on the periphery of the trap array. The next design would need to overcome this hurdle by giving each trap an equal likelihood of receiving an animal during loading and having trapping channel geometries that divert fluid and worms away from filled traps.

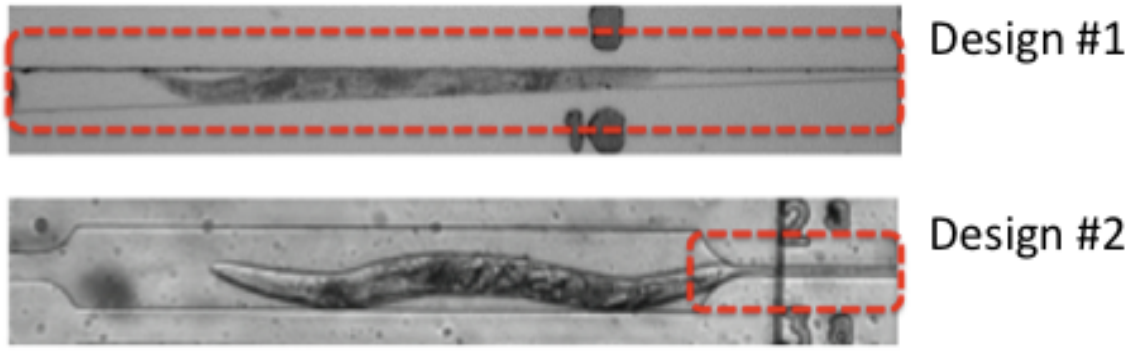

Figure 14: Comparison of Tapering Channels of Worm Traps. The red-dotted rectangle indicates the region of the traps that actually taper in width along the length of the worm's body. An L4 worm can fit its entire body inside the tapering trap channel of the design #1. In the membrane immobilization parallel trap device, version 1 (design #2), the tapering region at the end of the trap channel is short and abrupt; allowing only a small portion of the worm's tail to fit in the tapering region to block flow.

4.4 Design #3: Membrane Immobilization Parallel Trap Device (Version 2)

We developed a third device to further optimize the worm loading, trapping, immobilization, imaging, and laser nanoaxotomy based on the experiences with the previous two designs. We made the following modifications: (1) We widened the

immobilization chamber so that the membrane could sufficiently deflect to immobilize the animals. (2) We increased the length and tapering slope of the trapping channel so that the entire worm's body fits along the channel's length and blocks flow more effectively. (3) We arranged the immobilization chambers equidistant from the main inlet so that all traps had the same likelihood of receiving a worm. (4) We added a nutrient perfusion channel to go across all of the worm traps to sustain the animal viability over long periods of time on-chip. (5) Finally, we integrated a check valve at the entrance of each trapping chamber to prevent worms from exiting their chambers. These check valves do not require a pressurized membrane valve to stop animals from escaping the immobilization chamber. However, the complexity of the design made it difficult to include a bypass channel to flush out excess animals that did not enter one of the immobilization chambers.

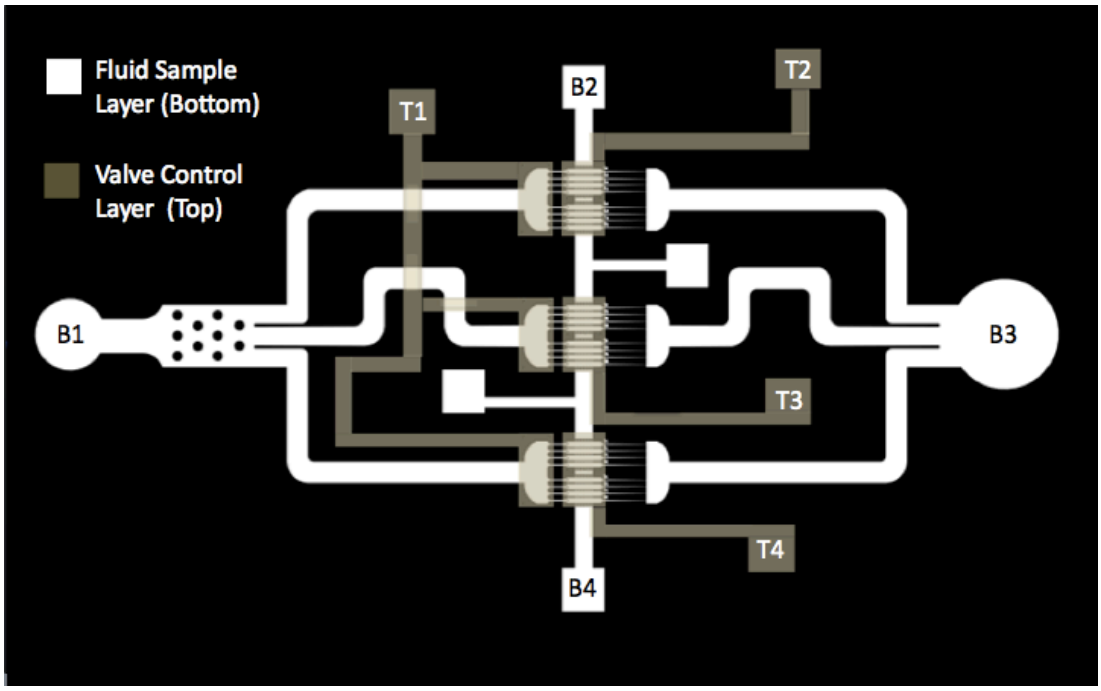

Figure 15: Design #3: Membrane Immobilization Parallel Trap Device (version 2). Worms and nutrient medium flow through the white channels, which are bonded to cover slip glass. The valve control layer (brown) is bonded on top of the thin PDMS layer above the white channels. The main worm-loading inlet is B1, which is followed by circular pillars to trap large debris and randomize flow so that an equal number of worms go to each of the three equal-length channels that branch off from this inlet. Each of these channels leads to eight worm traps for storage, imaging, and nanoaxotomy, followed by three equal-length channels to the main outlet (B3). B2 is the inlet for nutrient perfusion across the traps and eventually leads to the outlet, B4 on the opposite end of the vertical trap array. T1 controls three membrane valves at the entrance of the traps to prevent worms from escaping during long-term on-chip storage. T2-T4 control membrane valves for worm immobilization in the traps.

4.4.2 Design #3: Results

The traps dimensions are 1000 μm x 150 μm excluding the tapering channel region (Figure 16). Each worm trap is has check valve at its entrance to decrease the chance of worms escaping the trap over long periods of time (Figure 16). The check valve gap is 12 μm wide and is large enough for a 30 μm diameter worm to slip through

without visible damage to its body. The animal cannot exit the trap through this small gap without significant pressure applied from B3 to B1 (Figure 15). This is a safeguard to malfunctions of the membrane valve before the trap (T1). These modifications prevented all observed worms from escaping their traps after 72 hours on-chip.

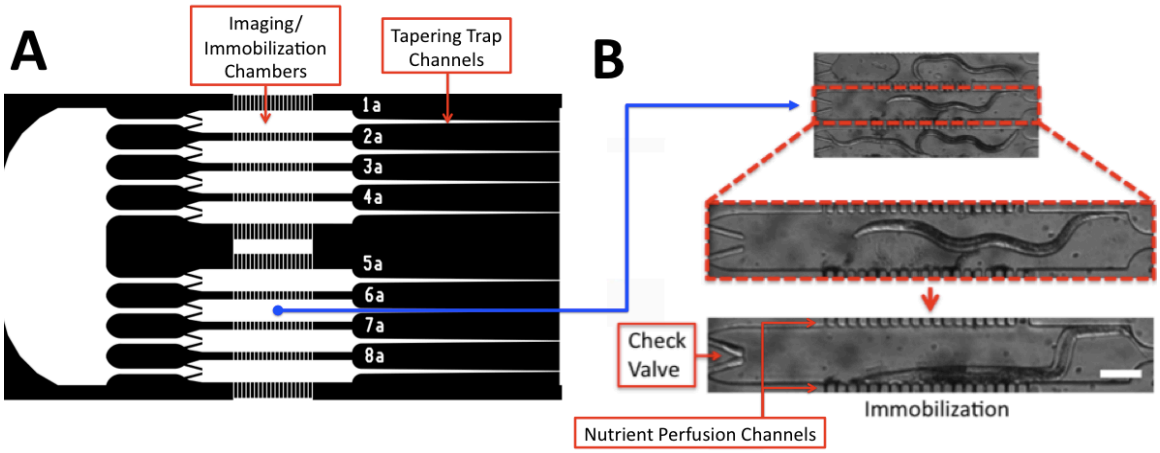

Figure 16: Function of a Single Trap in the Membrane Immobilization Parallel Trap (version 2). (a) One of the three immobilization chamber arrays with eight individual traps and tapering channels for initial trapping. **(b)** An individual trap with a single worm being immobilized by membrane deflection; each trap has a check valve at the entrance and a set of nutrient perfusion channels above and below the animal. (SCALE BAR ~100 µm)

The wider trap channel dimensions decreased the pressure required to immobilize the worms with the trapping membranes relative to the first membrane immobilization device. We also decreased the membrane thickness to ~5 microns to make it more deformable. These modifications made it so only ~103-138 kPa were required to completely immobilize the worms, whereas the 100 µm wide channels in the previous design required to 207-276 kPa and were not always capable of full immobilization. With the necessity of less force applied to their bodies by the membrane during imaging and

nano-surgery, the animals should be more viable over the course of multiple immobilizations.

4.4.3 Discussion: Design #3

The wider channel provided for better immobilization and allowed the worm to pirouette its body more freely. However, if the worm was in the process of undulating its body sinusoidally as the membrane is activated, there was a prossibility that one half of its body would be pressed against one side wall of the trap as the other half of its body was pressed against the opposite wall. The body section between the two halves was then crushed by the membrane (Figure 16b). Though we did not quantify how often this improper immobilization occurred, we observed increased worm mortality and body damage relative to the previous designs due to this device behavior. Thus, a mechanism to push the entire worm against only one of the trap's side-walls would greatly enhance the device's utility in nerve regeneration studies.

We believe that the nutrient perfusion channels had a deleterious effect on animal loading efficiency and function. As seen in Figure 17a, even though an animal could be stuck in the tapering channels and completely block flow across its body, unfilled traps on either side of that animal could provide a route for flow into the filled trap via the nutrient perfusion channels. Additional animals were able to hijack flow into traps with single or multiple animals during loading due to the existence of flow across the entrance of these filled traps to the nutrient perfusion channels and/or adjacent traps. The next iterations of this device should definitely avoid the nutrient perfusion channel in this

configuration. Non-essential channels can complicate device design and function in unexpected ways. Elimination of the nutrient channels in the next device, while still maintaining animal viability would be more optimal. For instance, nutrients could possibly be injected from the main device inlet at a low pressure or flow rate.

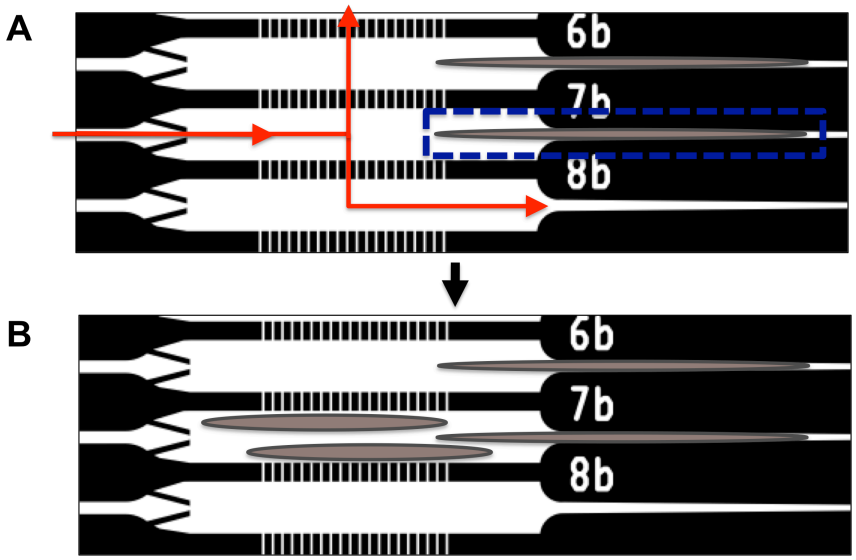

Figure 17: Worm Trapping Complications in Design #3. The nutrient perfusion channels made trapping a single worm in each chamber very difficult. **(a)** The red arrows illustrate possible routes for flow into the trap through the perfusion channels, despite the blockage of flow by an animal in the tapering region (blue square). **(b)** Multiple worms in a single trap.

4.5 Device Functionality Methods and Summary

We evaluated the functionality of three microfluidic devices designed to trap and immobilize multiple *C. elegans* worms in parallel for imaging and laser nano-surgery of their axons. We evaluated four main parameters in this study: (1) The animal loading time was essentially the time it took to load proportion of worms indicated in the second data column after the delivery of a single dose of 30-40 worms suspended in liquid to the

chip. (2) Percentage of traps filled is the proportion of the chip's immobilization chambers filled with one or more animals after the animal loading time. (3) We also evaluated immobilization capability in terms of the chip's ability to keep an animal completely still during imaging and surgery steps. If the animals moved it would be impossible to target their axons and obtain high-resolution images. (4) We finally looked at axotomy efficiency by seeing whether we could consistently cut axons with the chip in our optical setup after worm immobilization. These results are summarized in Table 1.

Table 1: Summary of Microfluidic Parallel Trap Device Performance

DEVICE \ PARAMETER	Animal Loading Time	Fraction of Traps Filled	Immobilization Possible	Axotomy Possible
Design #1: Single Layer Parallel Trap Device	< 1 min	~80-100%	Yes	No
Design #2: Membrane Immobilization Parallel Trap (Version 1)	~2-4 min	~50-60%	Inconsistent (due to thick membranes)	Inconsistent
Design #3: Membrane Immobilization Parallel Trap (Version 2)	~3-5 min	~40-60%	Yes	Yes

The single layer parallel trap device had the best performance in all categories except for the most crucial parameter to make the nerve regeneration studies feasible; axotomy efficiency. Once animals were trapped in the tapering channels, optical access to the axons was severely diminished and cuts with the fs-laser pulses at the energies used with our first microfluidic device (7-10 nJ) were nearly impossible. If we had increased

the laser energy to compensate for the energy loss due to scattering in tissue, we may have been able to perform axotomies.

The first membrane immobilization trap device (Design #2) improved upon the optical problems encountered in the single layer chip. However, the dimensions of the immobilization membrane prevented proper membrane deflection, which occasionally allowed the worms to move during imaging and surgery. The small membrane width may have also played a role. Without proper immobilization, targeting of axons was extremely difficult. Loading efficiency also decreased because we changed the layout of the chip to account for the membrane, which increased the spacing between immobilization chambers. Altering the tapering channel geometry also seemed to allow more than one worm to enter a single chamber by not permitting the worm's body to adequately block flow into the channel.

In the second version membrane immobilization trap device (Design #3), we could consistently immobilize animals and perform laser nanoaxotomy. However loading efficiency was decreased by the addition of a nutrient perfusion channel across the trap area. Having the traps fluidically connected to each other via this channel created unintended fluid flow profiles that allowed multiple worms to fill single traps, while preventing other traps on either side of the filled trap array to from receiving any animals.

Chapter 5: On-chip Neuroregenerative Studies of the D-type Motor Neurons and the PQR Neuron

Here we look at nerve regeneration of two different *C. elegans* neuron types in two separate chip designs. The first study looks at the regenerative capacity of the D-type motor neurons on the device developed by Guo *et al*. [10]. This investigation's purpose was to look at the feasibility of using fs-laser nanoaxotomy to cut these neurons on-chip with the membrane immobilization method, while observing the motor neurons' regenerative capacity, which may differ on-chip versus studies on agar pads with anesthetics.

The second study looks at regeneration of the PQR neuron's axon and dendrite processes using the membrane immobilization parallel trap device (version 2). This was simply a preliminary study to establish the capability of this device for nerve regeneration studies and to begin the investigation of the PQR neuron's regenerative capacity.

5.1 D-type Motor Neuron Regeneration Studies on-a-Chip

In this study we followed a total of 62 neurons that were severed in 6 worms using the microfluidic trap developed by Guo et al.; 53% of them regrew and reconnected to their targets [10]. Time-lapse imaging showed that this could occur 6 to 9 hours after surgery in the microfluidic device (Figure 18), whereas it had taken 12 to 24 hours on agar pads [2]. As was seen with touch neurons, anesthetics seem to hinder axonal recovery time [10]. It should be noted that unlike the touch neurons, the axons of the

motor neurons mostly reconnect to their target in the dorsal cord (Figure 19a) and rarely to the distal stumps. We classified an axonal reconnection as a true neuronal recovery when the axon reconnected to its specific distal partner on the dorsal cord. Because of the proximity of motor neurons to each other, we observed some cross-over, where axons reconnect to a neighboring process (Figure 19b). Since these aberrant reconnections did not reach their designated target, they were not counted among the axonal recoveries. Three hours after surgery, distal and proximal processes retract a few microns (Figure 18b), which was much shorter than the retractions observed in previous experiments [2]. The difference in energies used for axotomies (200 pulses of 15 nJ for this study instead of 100 pulses of 40 nJ) might explain this discrepancy.

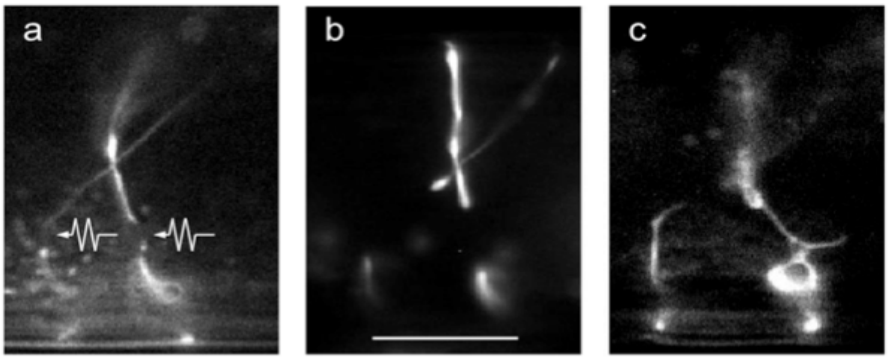

Figure 18: Time-lapse Imaging of Axonal Regrowth of Motor Neurons. (a) Axotomies were performed in two axons as indicated by the arrows using 200 pulses of 10 nJ pulse energy. **(b)** At 3 hours, both proximal and distal ends retracted for a few microns in both axons. **(c)** At 9 hours, both axons are reconnected. The picture was focused for the right axon. The present case of reconnection to the distal end is rather rare. On all pictures, the scale bar is 10 μm and the dorsal cord lies at the bottom.

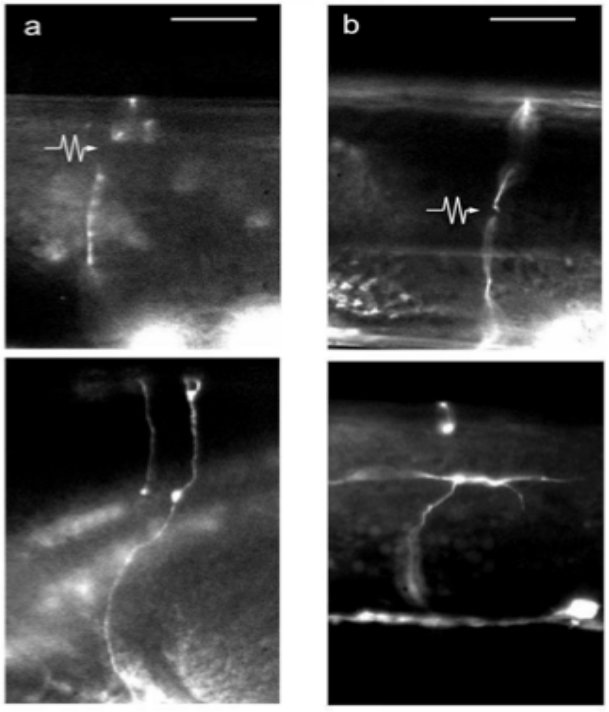

Figure 19: Different Types of Motor Neuron Axonal Recoveries. The pictures on the top row were taken immediately after axotomy. The arrows show where the axons were severed. The pictures at the bottom row were taken 9 hours after axotomy. **(a)** The regrowing axon directly reconnected to the dorsal cord process for most of the successful axonal recoveries (53% of the total operated neurons). The previous distal process is still visible on the left side of the new axon. **(b)** The misguided regrowing axon reconnects neither to the distal stump nor to its dorsal process. The scale bars are 10 μm. The dorsal cord is at the bottom.

Overall, we demonstrated that one could perform D-type motor neuron nerve regeneration studies with fs-laser nanoaxotomy on the described microfluidic platform. We were able to observe animals at multiple time points without the risks of long-term anesthetic exposure. We found that nerve regeneration in these axons was 3 to 15 hours faster than axons cut in worms on agar and anesthetics, which complemented a similar trend observed in mechanosensory neurons [2,10]. Further studies could look at a larger sample size of animals or mutant strains missing genes that affect the regeneration mechanisms, such as Ephrin and DLK-1 Kinase. It would also be beneficial to check whether the nineteen D-type motor neurons differ in their regenerative capacity based on their location along the anterior-posterior body axis.

5.2 Preliminary Regeneration Studies of the PQR Neuron on-a-Chip

We wanted to see if there was a difference in regeneration frequency and duration between the dendrite process and axonal process of the PQR neuron. Imaging and axotomies were performed on Design #3, and worms were stored in their traps until observation 12 hours later. The results are summarized in Table 2. As stated earlier, the strain used (*kyIs417*) expresses GFP in a subset of oxygen-sensing neurons, including PQR.

Table 2: Results on Regeneration Probability of PQR Neuron (on-chip). In this set of experiments we performed axotomies on either the axon or dendrite, and imaged the regeneration capability of the process 12 hours later.

Part of Neuron	Regrowth	Reconnection	No Growth
Axon	7/14, 50%	6/14, 43%	7/14, 50%
Dendrite	0/7, 0%	0/7, 0%	7/7, 100%

After 12 hours, we found that 50% of the axons cut exhibited some form of regrowth or reconnection, while the dendrites did not regenerate at all (Table 1). The most common morphology for axon regeneration was regrowth from a new process from the cell body that connected to the distal end of the original axon, as opposed to reconnection from the proximal stump created by the axotomy (Figure 20c & d). Our earlier studies showed that ventral cord process axotomies performed far away from the PQR cell body along the ventral cord did not regrow in any fashion after 12 hours.

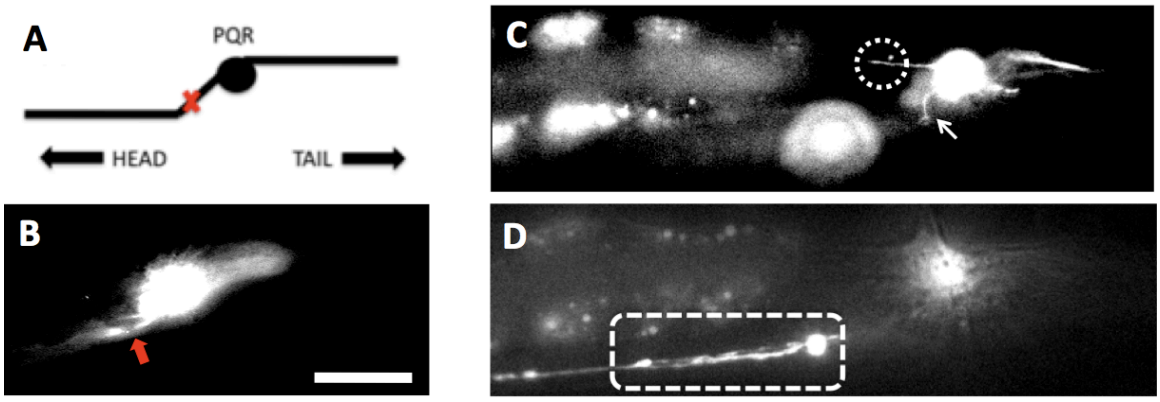

Figure 20: PQR Neuron, Regeneration of the Axon Process. (a) Schematic of fs-laser cut to the PQR neuron's axon process **(b)** PQR Neuron cell body and nanoaxotomy (red arrow) to the axon cord process (SCALE BAR ~10 µm). **(c)** 12 hrs later, the original axotomy site is just a proximal stump (white dashed circle), but a new ventral cord process has emerged from the cell body (white arrow). **(d)** (Same neuron and time point as (c), but a different focal plane) The new process in (c) has reconnected the distal axon, forming a bulbous structure (white dashed rectangle).

Additionally, we performed some axotomies on agar pads with anesthetics, which showed a 100% reconnection rate of the axon process 24 hours post axotomy. Additionally, these studies indicated that after 24 hours, the dendrite is also capable of regrowth ~50% of the time. These results suggest a need to perform additional on-chip studies on both PQR neuron processes over longer time scales. The difference in regeneration rate between axon and dendrite suggest a possible discrepancy in growth factor expression between their locations. It would also be interesting to investigate regeneration behavior when both processes are cut in the same neuron. Time-lapse imaging of the recovery process would reveal the morphology of how new proximal processes emerge from the neuron cell body.

Chapter 6: Conclusions and Future Directions

6.1 Conclusions

The studies described here demonstrate the increased feasibility of performing high-throughput studies of nerve regeneration in *C. elegans* using microfluidic platforms. We established that the on-chip deformable membrane immobilization method allows for adequate optical access for imaging and laser nanoaxotomy of two additional neuron types in *C. elegans*, D-type motor neurons and the PQR neuron. As previously shown in the ALM and PLM neurons, we observed neuronal recovery of the D-type motor neurons in the microfluidic device that was much faster than studies using anesthetics and agar for worm immobilization [2].

We demonstrated that this microfluidic membrane immobilization modality can be scaled up through parallelization of the fluidic channels that trap, immobilize, and house the worms, reducing the time and labor of performing these studies. Tests with the single layer parallel trap device demonstrated that multiple tapering channels in an array can quickly and easily trap many worms under pressurized flow, without overfilling any traps. While the tapering channels are useful for trapping single worms, they do not immobilize the animals in an orientation that allows for ideal optical access to the neurons. We decided to employ the double-layer microfluidic device principles in the first membrane immobilization parallel trap device and add an immobilization chamber and deformable membrane upstream of the tapering channels. However, we found that the dimensions of the tapering channel did not prevent multiple worms from filling the

individual traps. We also found that the width of the immobilization chamber needed to be expanded to allow sufficient deformation of the immobilization membrane to keep worms still for high-resolution imaging and surgery. We made these changes in the second version of this device and were able to perform ablation and imaging with ease. Between Design #2 and Design #3, we showed that increasing the width of the immobilization chamber and decreasing the membrane thickness greatly decreased the applied pressure required for immobilization. However, initial trapping of worms was also problematic, as the perfusion channels added in this design allowed multiple worms to fill a single trap, despite the fact an animal had already filled the trap's tapering channel.

6.2 Future Directions for Device Design

The next iteration of the parallelized microfluidic device should circumvent the uncertainties of worm loading and immobilization from the previous devices with a vastly different trap design. In Figure 21, we propose schematic of a possible the new worm trap design that could be part of an array of parallel traps. Before loading the worms into the trap, the valve control layer will deflect a membrane (brown) downward, so that no animals can pass the check valve. The channel upstream of this check valve is 40 μm wide and 1000 μm long, which will only fit one worm a time (Figure 21b).

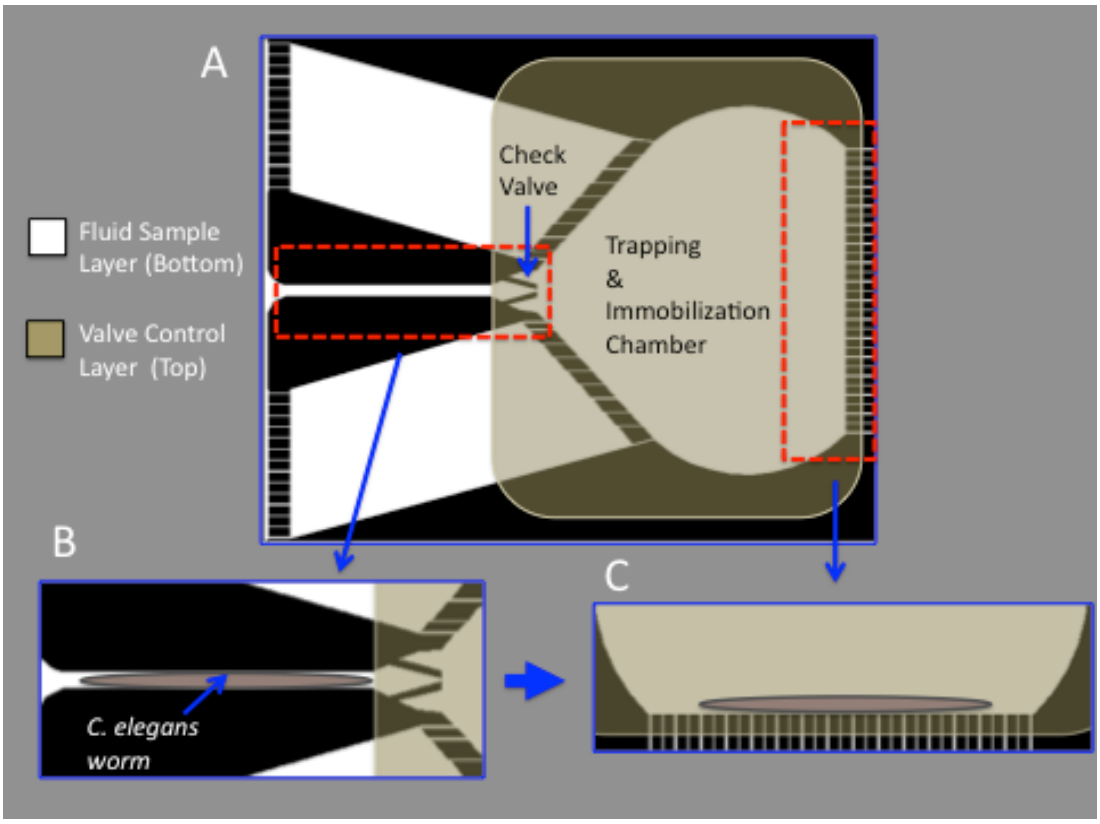

Figure 21: Schematic and Basic Function of a Single Trap in the Proposed Design. **(a)** The layout of a single immobilization chamber in the proposed device. **(b)** How initial trapping should happen through the worm-loading channel. **(c)** Worm immobilization in the immobilization chamber.

Once excess worms have been flushed from the chip, the valve control layer releases the membrane and the worm is immobilized against a small channel array, which is perpendicular to the applied flow. This configuration will straighten the animal against the back wall of the trap, against the sieve structure so that its body will not curve and be excessively damaged by membrane deflection, which was an issue encountered in Design #3.

We performed some fluid dynamic simulations of this immobilization chamber and saw the bulk of the fluid flow and the highest fluid velocities go right through the center of the back wall of the trap (Figure 22). The velocity vectors and fluid flow profile suggest that a majority of the fluid flux through the immobilization chamber will go to the center of the back wall sieve structure. This is where we would ideally want the animals to be immobilized. However, we are concerned about the circular flow profiles created on both sides of the bulk fluid flow to the center, as they may create a region where the animals may stall and the flow may be unable to pin the worms against the sieve structure (Figure 21c). We believe this profile is caused by the slower flow from the side channels being displaced by the bulk flow through the center. Yet, we are optimistic that the dynamic nature of the flow profile and a given worm's body movements would make it more likely that worms would be caught in the bulk flow that goes to the back wall. At that location, the membrane would not awkwardly immobilize the worms, as they did in Design #3. Actual experimental tests with the device would have to confirm these hypotheses.

Collectively, this new design attempts to integrate knowledge gained from the previous device iterations to make high-throughput nerve regeneration studies of *C. elegans* more feasible.

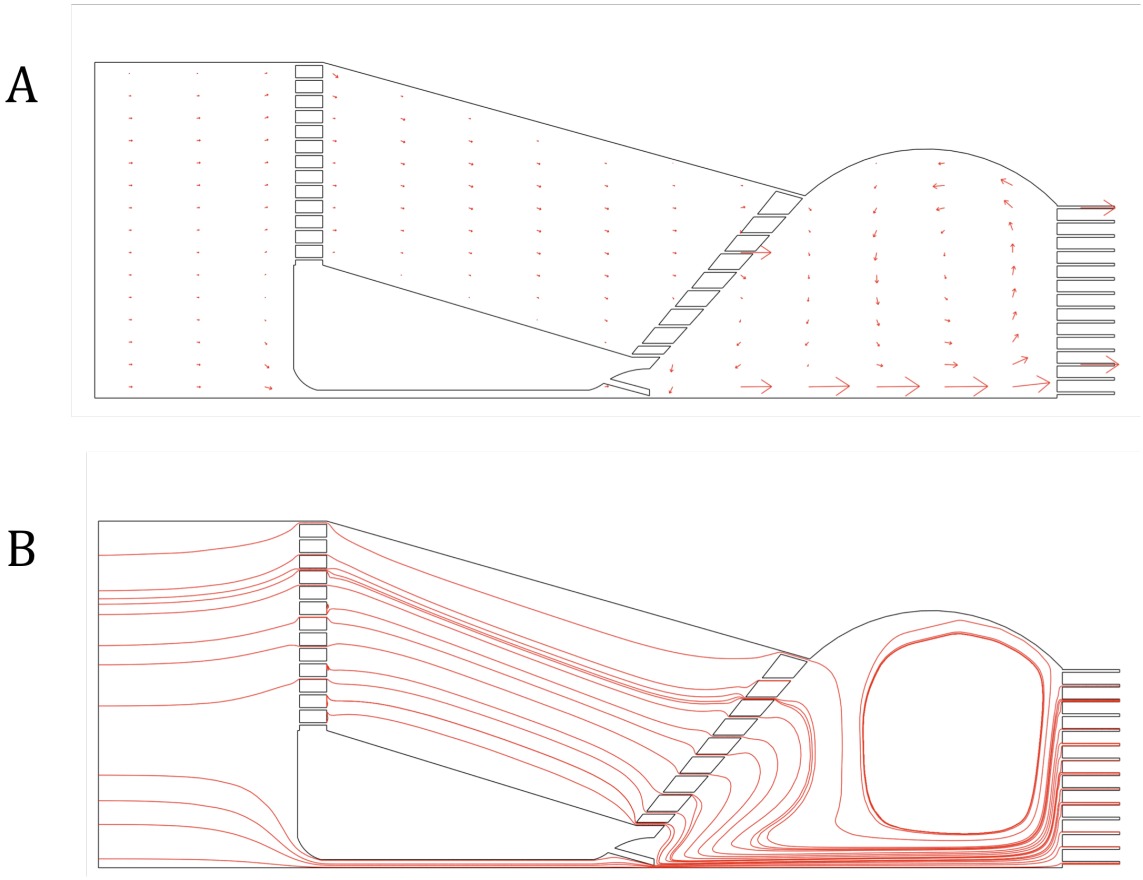

Figure 22: Fluid Dynamic Simulations of Proposed Worm Trap Design. (a) Two dimensional vector field of the fluid velocity. The largest velocities emerge from the center of the chamber through the worm-loading channel. **(b)** Flow profile simulation, a majority of the fluid flux goes through the center of the immobilization chamber to the sieve structure. (Note: In both (a) and (b), there is smaller fluid flux that flows circularly above the bulk flow moving to the back wall.)

References

[1] P.J. Horner and F.H. Gage, "Regenerating the damaged central nervous system.," *Nature*, vol. 407, 2000, pp. 963-70.

[2] M.F. Yanik, H. Cinar, H.N. Cinar, A.D. Chisholm, Y. Jin, and A. Ben-Yakar, "Neurosurgery: functional regeneration after laser axotomy.," *Nature*, vol. 432, 2004, p. 822.

[3] M. Kerschensteiner, M.E. Schwab, J.W. Lichtman, and T. Misgeld, "In vivo imaging of axonal degeneration and regeneration in the injured spinal cord.," *Nature Medicine*, vol. 11, 2005, pp. 572-7.

[4] D.H. Bhatt, S.J. Otto, B. Depoister, and J.R. Fetcho, "Cyclic AMP-induced repair of zebrafish spinal circuits.," *Science (New York, N.Y.)*, vol. 305, 2004, pp. 254-8.

[5] Z. Wu, A. Ghosh-Roy, M.F. Yanik, J.Z. Zhang, Y. Jin, and A.D. Chisholm, "Caenorhabditis elegans neuronal regeneration is influenced by life stage, ephrin signaling, and synaptic branching.," *Proceedings of the National Academy of Sciences of the United States of America*, vol. 104, 2007, pp. 15132-7.

[6] M. Hammarlund, P. Nix, L. Hauth, E.M. Jorgensen, and M. Bastiani, "Axon regeneration requires a conserved MAP kinase pathway.," *Science (New York, N.Y.)*, vol. 323, 2009, pp. 802-6.

[7] C.V. Gabel, F. Antoine, C. Chuang, A.D. Samuel, and C. Chang, "Distinct cellular and molecular mechanisms mediate initial axon development and adult-stage axon regeneration in C. elegans," *Development*, vol. 135, 2008, pp. 3623-3623.

[8] J. Melin and S.R. Quake, "Microfluidic large-scale integration: the evolution of design rules for biological automation.," *Annual review of biophysics and biomolecular structure*, vol. 36, 2007, pp. 213-31.

[9] K. Schuske, A.A. Beg, and E.M. Jorgensen, "The GABA nervous system in C. elegans.," *Trends in Neuroscience*, vol. 27, 2004, pp. 407-14.

[10] S.X. Guo, F. Bourgeois, T. Chokshi, N.J. Durr, M.A. Hilliard, N. Chronis, and A. Ben-yakar, "Femtosecond laser nanoaxotomy lab-on-a- chip for in vivo nerve regeneration studies," *Nature Methods*, vol. 5, 2008, pp. 531-533.

[11] C. Gonzalez, L. Almaraz, A. Obeso, and R. Rigual, "Carotid body chemoreceptors: from natural stimuli to sensory discharges.," *Physiological Reviews*, vol. 74, 1994, pp. 829-98.

[12] S.J. Araújo and G. Tear, "Axon guidance mechanisms and molecules: lessons from invertebrates.," *Nature Reviews Neuroscience*, vol. 4, 2003, pp. 910-22.

[13] C. Schmitz, P. Kinge, and H. Hutter, "Axon guidance genes identified in a large-scale RNAi screen using the RNAi-hypersensitive Caenorhabditis elegans.," *Proceedings of the National Academy of Sciences of the United States of America*, vol. 104, 2007, pp. 834-9.

[14] D. Yan, Z. Wu, A.D. Chisholm, and Y. Jin, "The DLK-1 kinase promotes mRNA stability and local translation in C. elegans synapses and axon regeneration.," *Cell*, vol. 138, 2009, pp. 1005-18.

[15] C.B. Rohde, F. Zeng, R. Gonzalez-Rubio, M. Angel, and M.F. Yanik, "Microfluidic system for on-chip high-throughput whole-animal sorting and screening at subcellular resolution.," *Proceedings of the National Academy of Sciences of the United States of America*, vol. 104, 2007, pp. 13891-5.
[16] K. Chung, M.M. Crane, and H. Lu, "Automated on-chip rapid microscopy , phenotyping and sorting of C . elegans," *Nature Methods*, vol. 5, 2008, pp. 637-643.
[17] S.E. Hulme, S.S. Shevkoplyas, J. Apfeld, and G.M. Whitesides, "A microfabricated array of clamps for immobilizing and imaging C . elegans," *Lab on a Chip*, 2007, pp. 1515-1523.
[18] P.B. Allen, A.E. Sgro, D.L. Chao, B.E. Doepker, J. Scott Edgar, K. Shen, and D.T. Chiu, "Single-synapse ablation and long-term imaging in live C. elegans.," *Journal of Neuroscience Methods*, vol. 173, 2008, pp. 20-6.
[19] M.W. Berns, W.H. Wright, and R.W. Steubing, "Laser Microbeam as a Tool in Cell Biology," K.W. Cytology, Academic Press, 1991, pp. 1-44.
[20] A. Vogel, J. Noack, G. Hüttman, and G. Paltauf, "Mechanisms of femtosecond laser nanosurgery of cells and tissues," *Applied Physics B*, vol. 81, 2005, pp. 1015-1047.
[21] B. Kirby, *Micro- and Nanoscale Fluid Mechanics: Transport in Microfluidic Devices*, NewYork, N.Y.: Cambridge University Press, 2010.
[22] J.C. Coates and M. de Bono, "Antagonistic pathways in neurons exposed to body fluid regulate social feeding in Caenorhabditis elegans.," *Nature*, vol. 419, 2002, pp. 925-9.
[23] C.I. Bargmann, "Chemosensation in C. elegans.," *WormBook : the online review of C. elegans biology*, 2006, pp. 1-29.
[24] N. Nguyen and S. Wereley, *Fundamentals and Applications of Microfluidics*, Boston, MA: Artech House, 2006.
[25] R. Shah and A. London, *Laminar Flows Forced Convection in Ducts*, New York, N.Y.: Academic Press, 1978.
[26] D. Hall, *C. elegans Atlas*, Cold Spring Harbor, N.Y.: Cold Spring Harbor Laboratory Press, 2008.

Vita

Navid Ghorashian was born on the Twelve of August, 1983 in Logan, Utah. He was raised in Mountain View, CA and Sunnyvale, CA, which are both in the southern part of the San Francisco Bay Area. Both of his parents were engineers and enjoyed successful careers in their respective fields. Navid attended Saint Francis High School in Mountain View, CA and graduated in 2001. Then he pursued a degree in Molecular and Cellular Biology with an emphasis in genetics at the University of California, Berkeley. While participating in research as an undergraduate, he developed an interest in the intersection of biology and engineering, eventually working on microfluidics for biological applications in the lab of bioengineering professor, Dr. Luke P. Lee. From there he worked for nearly a year at CellASIC Corporation in San Leandro, California, where he developed and tested microfluidic cell and tissue culture platforms for drug screening applications. Needing to come back to the diverse intellectual environment of a large university, Navid arrived at the University of Texas at Austin in the Fall of 2007, where he has been working under Dr. Adela Ben-Yakar in the Department of Biomedical Engineering. In Austin, he has focused on the development of microfluidic tools for high-throughput studies of nerve regeneration after axotomy by femtosecond pulse lasers in the roundworm *Caenorhabditis elegans*.